Economic Geology
Vol. 88, 1993, pp. 1483–1511

Oxygen Isotope Alteration in the Noranda Mining District, Abitibi Greenstone Belt, Quebec

L. M. CATHLES

Department of Geological Sciences, Cornell University, Ithaca, New York 14853

Abstract

A regional whole-rock oxygen isotope survey carried out in the Noranda district shows how oxygen isotope alteration can be used to guide exploration for massive sulfide deposits. The survey is based on 588 outcrop whole-rock oxygen isotope determinations from 478 sites in a ~35- by 50-km area between the Destor-Porcupine and Cadillac-Larder Lake breaks from east of the Horne mine to west of the Magusi River mine. The mean isotopic composition of all samples is 7.4 ± 2 per mil (SMOW). Nested analysis of variance of 478 isotopic determinations from 371 of these sites shows that 74 percent of the total variance in whole-rock $\delta^{18}O_r$ (r = whole rock) is associated with outcrop location, 21 percent with outcrop sampling, and 5 percent with sample analysis. An analysis of 259 determinations indicates that rock type is statistically no more important than outcrop sampling. The statistical analysis indicates that isotopic variations greater than ±1 per mil can be used to map the hydrothermal circulation responsible for massive sulfide mineralization. Specific traverses visually confirm the lack of ^{18}O dependence on rock type and the utility of a 2 per mil interpretive band. The large-scale pattern of isotopic alteration in the Noranda district is dominated by a nearly continuous 2- to 3-km-wide annulus at the margins of the Flavrian pluton of $\delta^{18}O_r < 6$ per mil (with values as low as 0.6‰). Six fingers of $\delta^{18}O_r < 6$ per mil radiate from the annulus. Five of the six point up section toward most of the massive sulfide deposits in the district, including two hosted by cycle IV (Dufault granodiorite-related) extrusions. The Flavrian $^{18}O_r$ depletion is surrounded up section by a ~10-km-wide band of patchy but intense ^{18}O enrichment (8.5–14‰). The combined pattern of concentric light and heavy alteration has a diameter of ~30 km. The Clericy intrusion shows a similar pattern of isotope alteration on a smaller (10 km diam) scale. The Lake Dufault pluton seems to have been isotopically altered by continuing convection driven by the Flavrian hydrothermal system. Modeling suggests that the ^{18}O depletion is produced by water circulating toward and along the edges of an intrusion, and that the surrounding heavy alteration is produced either by seawater recharge or limited hydrothermal discharge. The large scale and coherency of the alteration pattern centered on the Flavrian pluton is remarkable and indicates that this pluton drove a major, long-lived (~10 m.y.) hydrothermal system in which convection penetrated to an >8-km depth. The intensity and coherency of the ^{18}O depletion correlates with the tonnage of associated massive sulfide mineralization. Oxygen isotope depletion may in general mark the margins of plutons that have driven sufficient hydrothermal circulation to produce economic massive sulfide deposits up section. It may be possible to screen plutons for up-section massive sulfide exploration potential by collecting and isotopically analyzing ~50 samples from five traverses across a pluton's margins. Additional samples may provide details (light fingers) that guide exploration to particular deposits.

Introduction

PRESENT approaches to massive sulfide exploration such as geophysical anomalies and geochemical changes in alteration pipes apply only quite near the massive sulfide lenses. Coarse pyroclastics, rhyolite domes, disseminated pyrite in the volcanic stratigraphy, and hydrothermal alteration occur laterally within a kilometer or so of massive sulfide ore. Feeder pipes can be traced a kilometer or so below ore. Fallout from vent plumes (exhalite) is sometimes more broadly dispersed, but the dispersion pattern is subject to distortion by ocean currents. In some cases exhalite fallout is less dispersed than the footwall alteration (e.g., Kalogeropoulos and Scott, 1983).

Convective processes tend to focus hydrothermal discharge. On the other hand, the area of fluid recharge in a convection system is much greater than the area of discharge (Fig. 1). If the area of recharge or the pattern of subsurface circulation that fed discharge and produced massive sulfide deposits could be mapped, the dimensions of the massive sulfide exploration target might be increased an order of magnitude or more. The possibility of using oxygen isotope maps of a hydrothermal system to screen ~10- by 10-km areas for their exploration potential and to increase the size of the exploration target for particular deposits led the Chevron Oil Field Research Company to support the field test reported in this paper.

0361-0128/93/1493/1483-29$4.00

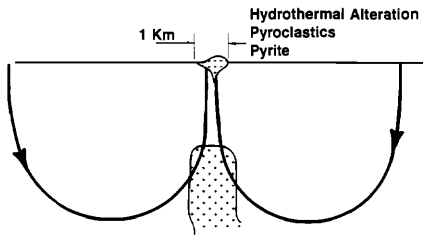

FIG. 1. Hydrothermal alteration, pyroclastics, and rhyolite domes are all localized by the same vents that focused the hydrothermal discharge to produce accumulations of massive sulfides. The objective of this field trial was to expand the exploration target by finding ways to map a larger part of the hydrothermal system. Accomplishment of this objective could increase the exploration target from ones to tens of kilometers.

Oxygen isotopes provide an ideal way to map geothermal systems:

1. Water is 90 wt percent oxygen.
2. Seawater contains far more ^{18}O than is in equilibrium with rock at low temperatures and thus "enriches" the rock in recharge areas.
3. Once water reaches isotopic equilibrium with rock at ~75°C, the equilibrium ^{18}O concentration in water increases strongly with temperature. Removal of rock ^{18}O thus occurs where seawater circulates up the geothermal gradient or toward an igneous intrusion. This temperature-dependent isotopic alteration outlines the hydrothermal heat source and produces other significant large-scale changes that map the deeper parts of the hydrothermal system.
4. Isotopic alteration is proportional to the amount of fluid circulation and therefore cannot easily be changed by subsequent metamorphism.
5. The intensity and volume of some of the isotopic alteration records the amount of water circulated and provides a quantitative measure of the potential of the system for massive sulfide mineralization.

Geology of the Noranda District

The Noranda mining district in the Abitibi greenstone belt was chosen for the test on the basis that it was a well-studied area, with unusually good outcrop exposure and low-grade later metamorphism.

The Abitibi greenstone belt is composed of about 12 separately erupted ellipsoidal volcanic sequences of extensive, thin, flat lava flows which Goodwin and Ridler (1970) refer to as volcanic complexes. One of these is the 200- by 50-km Noranda-Benoit volcanic complex. This complex plunges to the east and is composed of two and one-third major compositional cycles called supergroups. Each supergroup consists of basal komatiites overlain first by tholeiites and then by calc-alkalic extrusions (Jensen and Langford, 1985). Centers of volcanic eruption ~30 km in diameter are indicated in the later stages of each megacycle by rhyolite intrusions and extrusions (Goodwin and Ridler, 1970), locally intense volcano-tectonic activity, thickness changes in volcanic units, an increase in the ratio of sheet to pillowed mafic lava flows, an increase in magma vesicularity and volcanic breccia, a domal structure with comparatively little deformation (Dimroth et al., 1982), and synvolcanic, multiphase tonalitic-trondhjemitic intrusions with negative gravity anomalies (Goodwin and Ridler, 1970; Goodwin, 1977). Massive sulfide mineralization is associated with the centers of volcanic eruption. The Noranda massive sulfide district is the center of volcanic eruption in the Noranda-Benoit volcanic complex.

Massive sulfide deposits in the Noranda district are hosted by the Blake River Group, the 12- to 15-km-thick calc-alkaline member of supergroup III (the last supergroup erupted; Gibson and Watkinson, 1990). The Destor-Porcupine break separates the Blake River volcanics from the earlier tholeiitic phase of supergroup III (the Kinojevis volcanics) to the north (Fig. 2). The Cadillac-Larder Lake break separates the Blake River volcanics from Proterozoic and Archean sediments to the south. Reflection seismic profiles show these breaks to be near-vertical faults extending to depths of 9 to 16 km and that the Moho lies at a 35- to 38-km depth (Green et al., 1990). Similarities with the Kapuskasing uplift section suggest that 6 to 13 km of greenstones overlie a midcrustal layer of intraplated tonalites and a lower layer of mafic and anorthositic rocks (Green et al., 1990).

Most of the cycle III volcanics at Noranda were erupted extremely rapidly in a 5-m.y. period of crustal extension between 2703 and 2698 Ma (Corfu, 1993). The tholeiitic flows of cycle III (the Kinojevis) spread out extensively over flat terrain. Aeromagnetic surveys show alternating bands of high and low magnetic intensity that are continuous over distances of more than 100 km. The bands correspond to Fe- and Mg-rich volcanic flows (Letros et al., 1983). The calc-alkaline Blake River volcanics that form the Noranda complex are composed of many small overlapping and coalescing extrusive flows. Andesite flows are ~6 to 120 m thick and can be traced for up to 6.5 km. Rhyolite flows are ~30 to 360 m thick and can be traced for 10 km. "The volcanism is envisaged as the quiet outpouring of lava sheets on to the sea floor from magma rising through numerous fissures and small vents, the outpourings interrupted by periods of quiescence" (Spence and de Rosen-Spence, 1975, p. 94). Space for the extrusive flows was in part provided by synvolcanic subsidence associated with magma withdrawal (Gibson and Watkinson, 1990).

The Blake River Group volcanics erupted from the Noranda center of volcanism in five mafic-felsic cycles. The volcanics dip east and the mafic members show a consistent REE evolution up section (Gelinas

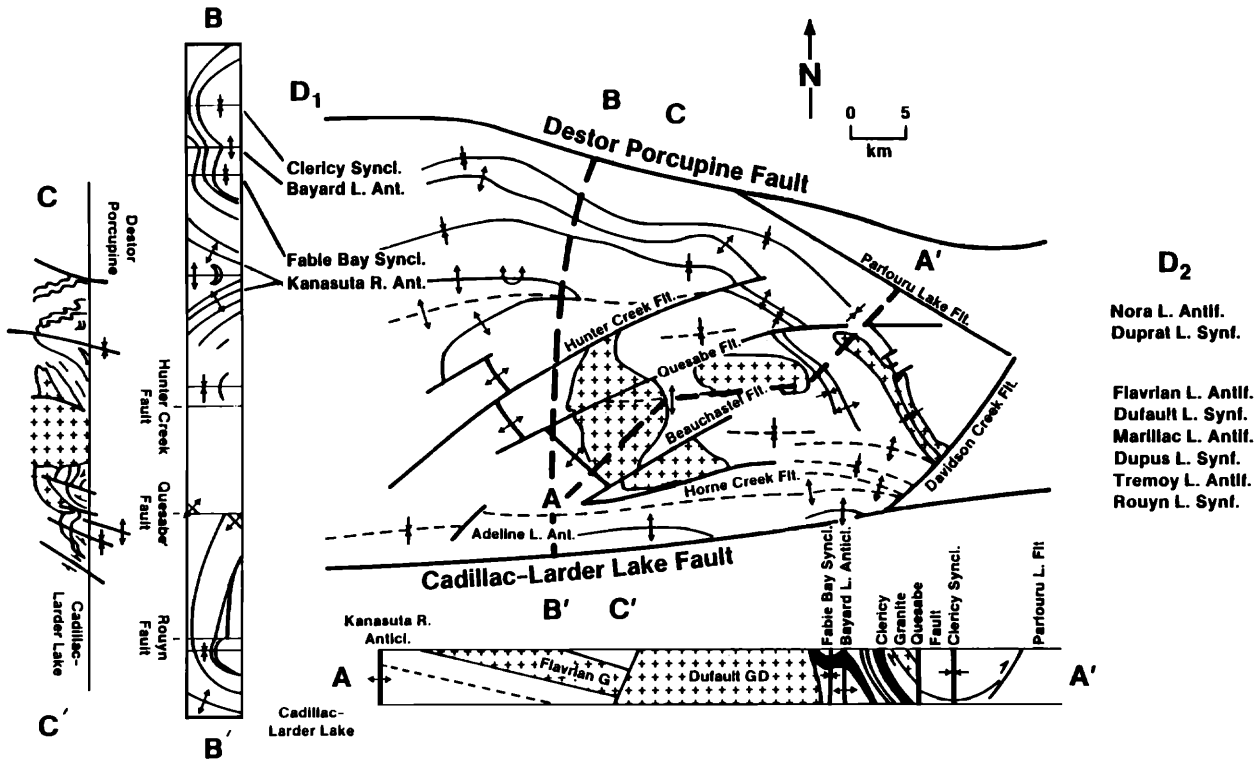

FIG. 2. Structural mapping shows two periods of deformation (D_1 and D_2). Northeast-trending faults downdrop the stratigraphy to the north. As discussed in the text the Flavrian pluton shown in cross section A-A' may be a felsic cap on a large mafic intrusion. This figure is simplified from Hubert et al. (1984). Abbreviations: ant, anticl = anticline, antif = antiform, flt = fault, G = granite, GD = granodiorite, L = lake, syncl = syncline, synf = synform.

and Ludden, 1984). A composite felsic intrusion is associated with most of the cycles. These intrusions (shown in section A-A' in Fig. 2) have been radiometrically dated. The Flavrian Lake pluton (cycle III) has an age of 2700.3 ± 1.3 Ma (Vervoort et al., 1993), the Dufault granodiorite (cycle IV) is 2690 Ma, and the Clericy pluton (cycle V) is 2684 ± 1 Ma (Corfu, 1993). The plutons generally produce relatively sharp negative gravity anomalies, but the anomalies are not large enough to allow the plutons to extend below a 5- to 15-km depth. The plutons are thought to be felsic caps on denser mafic bodies (Goodwin, 1977).

Kerr and Gibson (1993) review the distribution of massive sulfide deposits in the Noranda district. Most of the massive sulfide deposits at Noranda are hosted within the cycle III Mine sequence volcanics and are thought to have been produced by hydrothermal circulation driven by the cycle III Flavrian Lake pluton. Only a few are associated with the Dufault granodiorite of cycle IV and the Clericy pluton of cycle V. The Mine sequence volcanics and Flavrian Lake pluton were emplaced during the phase of rapid crustal extension discussed by Corfu (1993), whereas the later intrusions and extrusions were emplaced after the onset of the ensuing compressive phase. This compression caused some faulting and deformation of the volcanic pile. Northeast-trending faults cut the Flavrian and Lake Powell granites as indicated in Figure 2. From north to south these are the Hunter Creek, the Quesabe, the Beauchastel, and the Horne Creek faults. Downdrop occurs on the northwest side of the faults (Hubert et al., 1984).

The volcanism was clearly associated with rifting (crustal extension). The breaks may have resulted from the docking of fragments of oceanic plateau (Vervoort et al., 1993) or the closing of a marginal basin (Corfu, 1993). The centers of volcanic eruption are generally much less structurally deformed than their surroundings as if the volcanic activity strengthened and made them more resistant to deformation. The Mine sequence rhyolites and associated mafic volcanics to the east and north of the Flavrian pluton today dip to the east and north at 30° to 80°. Sampling along this horizon provides cross-section profiles. The area to the west of the Flavrian granite is the footwall of that intrusion; the area to the east, the hanging wall. Deformation along the breaks can be

intense, and the breaks were intruded by alkalic intrusions and were sites of alkalic extrusive activity at the end of supergroup III volcanism (e.g., Jensen and Langford, 1985).

The breaks are the main host for gold deposits, whereas massive sulfide deposits occur mainly between the breaks. Many of the break gold deposits at Noranda are associated with a late hydrothermal pulse that occurred between 2625 and 2600 Ma (Corfu, 1993) and which also reset Pb-Pb but not U-Pb ages in the Blake River volcanics (Vervoort et al., 1993). Pore fluid expulsion associated with the compression may account for the hydrothermal pulse (Corfu, 1993).

The association of the Noranda massive sulfide deposits with an episode of rapid crustal rifting and their striking similarity to kuroko massive sulfide deposits in Japan and to massive sulfide deposits on the ocean floor, suggests that they formed by seawater convection driven by rift intrusions (Cathles et al., 1983). If so, perhaps the most important factors favoring mineralization are the extremely large eruptive volumes discharged from the Noranda volcanic center and the unusually thick crust. There were several cycles or pulses of volcanism, however, and several felsic plutons mark the eruptive centers of the volcanic pile. Most of the mineralization is associated with only one of these plutons and one particular volcanic cycle. The specific exploration issues that must be addressed by the field test are therefore whether oxygen isotopes can identify the main (most prospective) volcanic cycle and point to massive sulfide mineralization within that cycle.

The Expected Pattern Of Isotopic Alteration

Computer calculations indicate the expected pattern and causes of large-scale, whole-rock oxygen isotope alteration. Models afford a basis for the planning and interpretation of the field study by providing a complete and concrete prediction of the alteration pattern of $\delta^{18}O_r$ (r = whole rock) values associated with massive sulfide mineralization on a 15-km scale. It is unlikely that a field test of the magnitude described could have been undertaken in the absence of these concrete predictions.

Computer models of oxygen isotope alteration have been published by a number of authors (e.g., Norton and Taylor, 1979; Parmentier, 1981; Cathles, 1983; Bowers, 1985). Even though the models are quite different in their chemical and kinetic assumptions, all predict $^{18}O_r$ depletion near the edges of intrusive bodies. This concurrence reflects the importance of the temperature dependence of the isotopic fractionation factor which expresses the difference between the whole-rock oxygen isotope composition and the oxygen isotope composition of the water in equilibrium with that rock, $\delta^{18}O_r - \delta^{18}O_f$ (f = fluid). The most chemically realistic model developed to date ties isotopic alteration to the mineralogical changes that occur during stepwise heating and progressive reaction of seawater with fresh basalt (Bowers and Taylor, 1985). The chemical changes are predicted by the chemical reaction code EQ6. The model is unrealistic in some regards; for example, it assumes that fluids interact only with fresh basalt and that product minerals remain in equilibrium with the hydrothermal fluids throughout the alteration. Thus changes in $^{18}O_r$ and mineralogic changes are not allowed to affect the evolution of isotopic alteration. Bowers and Taylor's analysis shows, however, that when chemical and isotopic alteration are coupled, pluton-driven convection produces $^{18}O_r$ enrichment at low temperatures and $^{18}O_r$ depletion in volumes of ~350°C fluid-rock interaction. They deduce an effective whole-rock fractionation curve that can be used to describe rock alteration in models that take into account the influence of early on later isotopic alteration as discussed below.

Figure 3 shows how a small pluton intruded at 700°C into a permeable environment will cause pore waters in the surrounding areas to convect and cool the intrusion. Figure 4 shows the oxygen isotope composition of the pore fluids during the convective cooling, whereas Figure 5 shows predictions of the oxygen isotope alteration of the rock that this fluid circulation will produce. The isotopic model used in the calculations in this paper determines the whole-rock alteration, taking into account the kinetics of isotopic alteration and using a temperature-dependent (but mineralogy-independent) fractionation factor determined from laboratory basalt alteration experiments (Cole, 1980). Details of the model calculations are given in Cathles (1983).

The temperature dependence of the fractionation factor is the most important model parameter, but the model is robust to variations in it. We have verified (but do not show here) that the calculated $\delta^{18}O_r$ values are similar for the whole-rock fractionation curve suggested by Bowers and Taylor (1985, fig. 14) and Cole's experiments, for example. Because of the simplifying assumptions in Bowers and Taylor's calculations it is not clear which fractionation factor is most appropriate. The calculated $\delta^{18}O_f$ values in lower temperature areas (<~150°C) would be ~5 per mil less negative if the Bowers and Taylor fractionation factor were used because their fractionation factor is offset from Cole's by about this amount. But so long as the isotopic fraction between water and rock decreases with increasing temperature, the $^{18}O_r$ patterns calculated by the model are similar for a wide range of kinetic and other factors. The pattern of $^{18}O_r$ alteration is what is important in the present discussion.

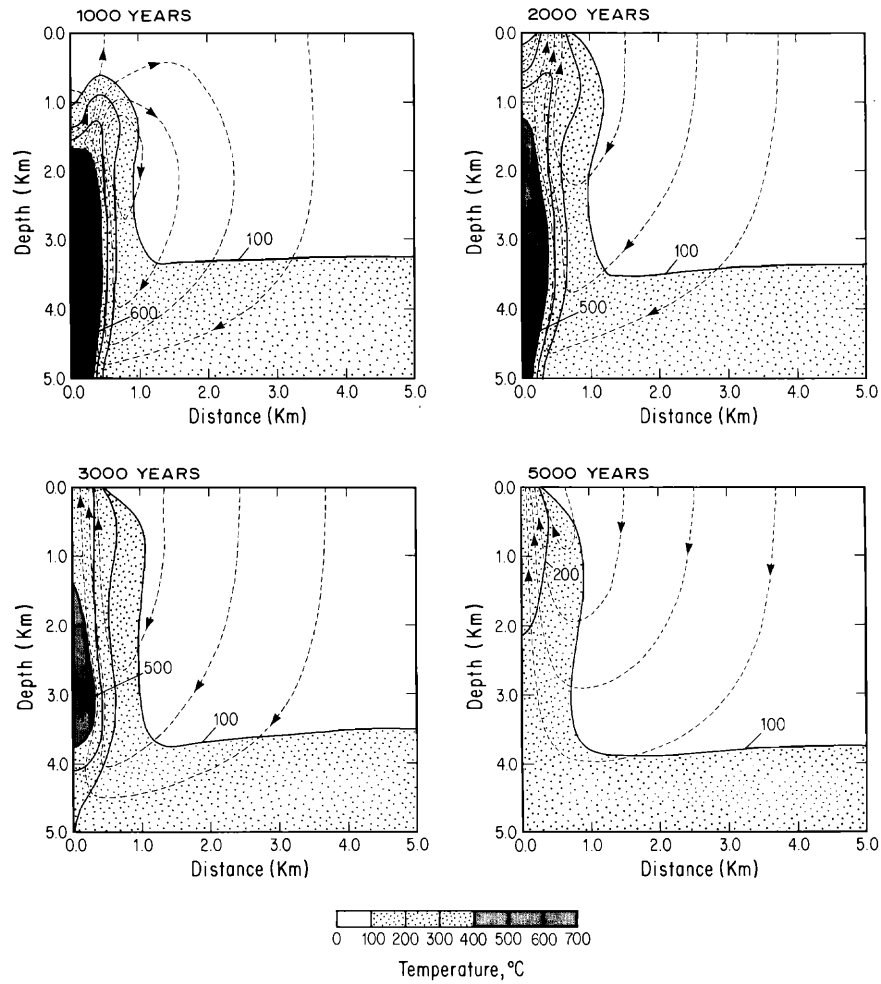

FIG. 3. Calculations showing, in cross section, the cooling of a small 3.25-km high, 0.5-km half-width intrusion at the left-hand side of the diagram by pore fluid convection. Time in years after intrusion is given for each section. Areas where temperatures exceed 100° and 400°C are shaded. Streamlines show the direction and velocity (faster when streamlines are bunched) of the fluid convection. The permeability of the intrusion and host rock is assumed to be 5 millidarcies at $T \leq 300°C$, but is exponentially reduced at temperatures above 300°C. Details of the calculations in this and the following two figures are given in Cathles (1983).

The temperature dependence of the fractionation factor provides the key to understanding much of the calculated alteration. The water and rock are very close to isotopic equilibrium in Figures 3 and 4 where the temperature exceeds ~75°C. In these equilibrium areas, isotopic alteration of the rock results from the temperature dependence of the rock-water fractionation factor and the circulation of water through a temperature gradient. For example, as the fluid convects to hotter temperatures, the fractionation factor decreases and the water becomes isotopically heavier (Fig. 4). The ^{18}O needed to make the water isotopically heavier is taken from the rock, which consequently becomes depleted in ^{18}O (isotopically light). Where water circulates up a thermal gradient in isotopic equilibrium with rock, the rock is depleted in ^{18}O. Conversely, where the water circulates down temperature in equilibrium with rock, the rock is enriched in ^{18}O. The light anomalies in rocks at 3-km depth and at the margins of the intrusion are the result of equilibrium isotopic exchange as fluids move up a temperature gradient. The heavy anomaly in rocks above the intrusion is the result of equilibrium isotopic exchange as fluids move down a temperature gradient.

The heavy, near-surface isotope anomaly that develops in rocks where seawater circulates into the rock formation (recharge) has a different explanation. Here the temperatures are below 75°C and the rate of isotopic alteration is controlled by the kinetics

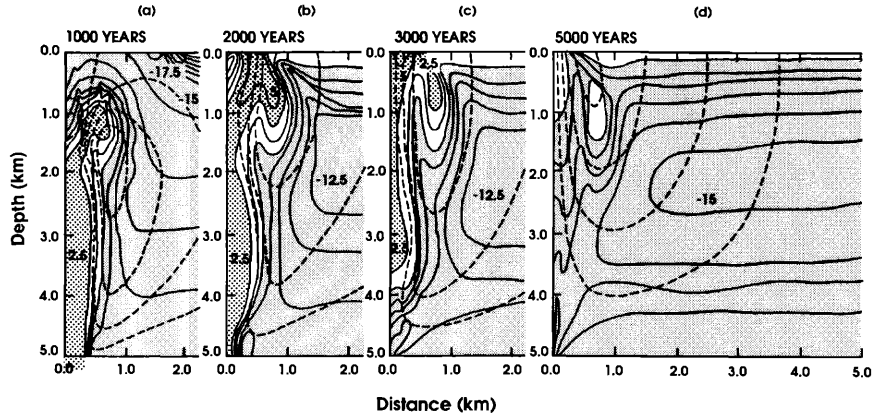

FIG. 4. Oxygen isotope composition of the fluid circulated in Figure 3. Seawater with $\delta^{18}O_f = 0$ per mil can be seen moving into the rock formation in recharge areas. Water-rock equilibration causes the $\delta^{18}O_f$ to drop to ~ -10 per mil 2.5 km below the recharge areas and to increase again to positive values as it interacts with the hot intrusion. The early hydrothermal ($\sim 350°C$) vent fluids are isotopically heavy ($\sim 5‰$), later hydrothermal vent fluids are ~ 0 per mil, becoming negative as the discharge wains and the discharge temperatures fall. Changes in the isotopic composition of the fluid combine with the movement of the fluid to produce the rock isotopic alteration shown in Figure 5. Patterns: coarse stipple = $\delta^{18}O_f >$ 2.5 per mil, fine stipple = $\delta^{18}O_f < -2.5$ per mil.

of isotopic exchange. The disequilibrium is caused by the 0 per mil composition of seawater, which is far heavier than the water that would be in equilibrium with rock at low temperatures. As convection continues, however, the rock near the surface gradually shifts to heavier isotopic signatures so as to be in equilibrium with 0 per mil water. Isotopically unshifted seawater can then penetrate to greater depths, so the surface anomaly with heavy $\delta^{18}O_r$ values grows with time. The surface rock anomaly thus measures the amount of water that has convected into the rock formation. It might be noted that if the water entering the system were meteoric water rather than seawater and had a $\delta^{18}O_f \sim -10$ per mil rather than ~ 0 per mil, the intensity of the near-surface rock anomaly would be reduced, but the oxygen isotope alteration pattern in the rest of the system would be unchanged.

On the basis of calculations such as those illustrated in Figures 4 and 5, the feeder pipes of massive sulfide deposits would be expected to have variably shifted $\delta^{18}O_r$ values but would generally be depleted in ^{18}O with respect to surrounding areas. The $\delta^{18}O_r$ values of the feeder pipes will depend on the time the venting terminated. If it terminates early, the feeder pipes will be isotopically heavy; if late, isotopically light.

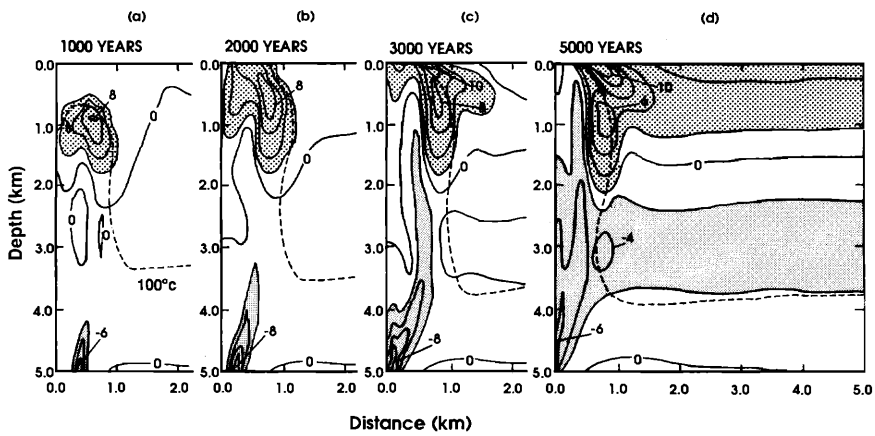

FIG. 5. The shift in whole-rock oxygen isotope composition caused by the circulation of water shown in Figure 4. Light whole-rock isotope anomalies develop at the margins of the intrusion and at depths of ~ 3 km where the waters recharge. Heavy whole-rock oxygen isotope alteration occurs near the surface in recharge areas and, initially, over the top of the intrusion. The pattern of isotopic alteration is distinctive. It is this pattern that may be utilized in massive sulfide exploration.

If the hydrothermal system operates as the volcanic pile accumulates and feeder pipes remain conduits of flow, the feeder pipes of massive sulfide deposits higher in the section will tend to be heavier. Feeder pipes and massive sulfide deposits should be surrounded in the hanging wall by a fugitive halo of ^{18}O enrichment. This halo will have a greater tendency to be preserved if the deposit formed toward the end of the hydrothermal event (high in the stratigraphy).

Recharge areas surrounding deposits should develop a very characteristic zonation in which ^{18}O enrichment of rocks within a few kilometers of the paleosurface overlie a layer of ^{18}O depletion and a deeper layer in which there has been little fluid circulation and little isotopic shift. Deposits deeper in the pile will tend to be surrounded by isotopically lighter rock both because there is more time for the prong of ^{18}O depletion growing upward from the intrusion to pass through the deposit's plumbing system, and there is time for isotopic alteration associated with deeper inflow to overwrite earlier heavy alteration. The margins of a stable magma conduit (some pluton margins) should become progressively depleted in ^{18}O.

Observations confirm the model patterns. Massive sulfide vents have been known for some time to be variably shifted isotopically. As summarized by Larson (1984), some massive sulfide feeder pipes have $\delta^{18}O_r$ values similar to their unaltered host-rock formations (5–8‰), some are enriched relative to the unaltered host, and some are depleted. Hoy (1993) shows that isotopic alteration near massive sulfide deposits at Noranda increases with stratigraphic level.

The fluids that cause feeder pipe alteration have a $\delta^{18}O_f$ value near 0 per mil. For example the Amulet A fluids have $\delta^{18}O_f = 0.5 \pm 1.0$ per mil (Beaty and Taylor, 1982). The vent fluids at the Matagami Lake mine have $\delta^{18}O_f = 1.5 \pm 1.0$ per mil (Costa et al., 1983). The vent fluids at the Fukazawa deposit in Japan increased from −6 to +4 per mil before decreasing to ~0 per mil during the later parts of the main massive sulfide deposition (Pisutha-Arnond and Ohmoto, 1983), in very good agreement with the model in the previous section (Cathles, 1983). The $\delta^{18}O_f$ values of the vent fluids for massive sulfide deposits in the Spanish pyrite belt were positive (Munha et al., 1986). At Crandon, Wisconsin, the feeder pipes were altered by a fluid with $\delta^{18}O_f \cong 0$ to −2.1 per mil (Munha et al., 1986). Hoy (1993) estimates that the fluids responsible for alteration near massive sulfide deposits at Noranda had $\delta^{18}O_f$ values that ranged from −2 (Corbet) to ~3.6 per mil (Horne).

In many areas, heavy intake isotopic alteration surrounds massive sulfide deposits at distances of ~5 km. Barriga and Kerrich (1984) found extremely high $\delta^{18}O_r$ values (up to 18‰) around massive sulfide deposits in the Spanish pyrite belt. Green et al. (1983) documented isotopic enrichment to 19.6 per mil peripheral to massive sulfide deposits in the Hokuroku district in Japan. The isotopic enrichment halo in Japan corresponds to zones of low-temperature (zeolite) alteration. The halo extends up to 5 km from the massive sulfide deposits. Both the magnitude of the isotopic enrichment and the dimensions of the halo agree with the model predictions (Fig. 5d).

A complete isotopic profile has been obtained through the Samail Ophiolite in Oman which contains several massive sulfide deposits (Gregory and Taylor, 1981). Strontium isotope enrichment clearly indicates that the cause of the isotopic alteration was the circulation of seawater into the rock formation. The seawater convection was presumably caused by intrusive activity related to crustal spreading in a marginal basin. The profile ranges from ~12 per mil (6‰ enrichment) near the sea floor, to ~3 per mil (3‰ depletion) at a 2- to 3-km depth, to unaltered values of ~5.7 per mil at still greater depths. The Samail profile matches nearly perfectly, both in the magnitude of the isotopic shifts and the depths at which the shifts occur, the intake zonation (heavy to light unshifted) shown to the right of the intrusion in Figure 5d. Profiles through ophiolites in Italy and Cyprus overlap parts of the Samail profile (Spooner et al., 1974, 1977a, 1977b). Profiles from the Archean Barberton greenstone belt are also similar (Hoffman et al., 1986).

Beaty (1980) showed that $\delta^{18}O_r$ values commonly increase by ~6 per mil from the mafic base to the felsic top of mafic-felsic volcanic cycles in the Abitibi greenstone belt. The isotopic shifts were caused by hydrothermal alteration not magmatic differentiation or contamination because relic pyroxene and quartz have normal magmatic $\delta^{18}O_r$ values (Beaty, 1980; Beaty et al., 1988) and because shifts of more than ~1 per mil are not expected as a result of magmatic differentiation (James, 1981). Paradis et al. (1993) document a very regular increase in $\delta^{18}O_r$ values over the Mine sequence section from the Flavrian to east of the Vauze massive sulfide deposit. Three traverses across the stratigraphy in a 3- by 3-km area east of the Vauze all show remarkably consistent up-section increases in $\delta^{18}O_r$ values.

The edges of intrusions that have driven significant hydrothermal systems have margins depleted in ^{18}O. Taylor (1974) noted that ground-water convection produces light isotopic alteration at the margins of intrusions with $\delta^{18}O_r$ values of 0 per mil or less (e.g., Forester and Taylor, 1977) and suggested that such isotopic halos might be useful in mineral exploration. An ^{18}O-depleted zone ~1 km wide and ~10 km long is immediately adjacent to a portion of the Mule Mountain trondhjemite in the West Shasta district. A protuberance in the middle of this light alteration band extends up section toward the Iron Mountain

massive sulfide deposit, the largest in the district. The light alteration at the edges of the Mule Mountain trondhjemite is surrounded at distances of ~5 km by areas with $\delta^{18}O_r > 9$ per mil. These patterns are indicated by a survey of about 60 $\delta^{18}O_r$ determinations over a 20- by 25-km area (Taylor and South, 1985). Similarly, a survey of more than 100 $\delta^{18}O_r$ determinations over a 15- by 20-km area of the Solea graben (a fossil spreading center) in the Troodos massif in Cyprus shows a light prong of $\delta^{18}O_r$ alteration extending upward from a zone of epidosite alteration to the feeder pipes of the 15×10^6-metric ton Mavrovouni and 6×10^6-metric ton Skouriotissa massive sulfide deposits (Schiffman and Smith, 1988). The light $^{18}O_r$ alteration is surrounded by heavy $^{18}O_r$ alteration that is concordant with the ophiolite pseudostratigraphy, but the light $^{18}O_r$ alteration cuts sharply across that stratigraphy. Schiffman and Smith suggest that the heavy alteration is caused by diffuse seawater recharge and the light alteration by focused hydrothermal venting that carries metals from their source in the epidosites to their sites of deposition in the up-section massive sulfide deposits.

Isotopic investigations of the alteration caused by pore water convection around igneous intrusions thus strongly support the general predictions of the simple convective-isotopic alteration model shown in Figures 4 and 5 and strongly suggest that oxygen isotopes can be used to map hydrothermal systems responsible for massive sulfide mineralization and perhaps even guide exploration to specific massive sulfide deposits.

Sampling and Analysis Procedures

Five hundred and two new surface samples were collected between 1983 and 1987 from 452 sites in a ~35- to 50-km part of the Noranda massive sulfide district bounded by the Destor-Porcupine and Cadillac-Larder Lake breaks and extending from east of the Horne mine to west of the Magusi River mines. From 1983 to 1985 the samples were collected in a fashion that could support a nested analysis of variance. That is, multiple isotopic analyses were made of many samples (60 replicate analyses total), multiple samples were collected from many sites (50 replicate site samples total), and the rock type was noted. A nested analysis of variance was then used to allocate the percentage of total variance between regional location, sampling location at a particular site, rock type, rock crystallinity, and analytical error. After 1985 only one sample was collected from each outcrop. Oxygen isotope analyses from an additional 26 sites reported by Beaty (1980) were incorporated in this study. The total number of sites was thus 478 and the total number of isotopic determinations 588. All are tabulated in the Appendix.

Sampling of the unjointed parts of outcrops proved difficult. However, the few chips we were able to extract generally were isotopically similar to those extracted near joints. The sampling and analysis procedure was as follows:

1. In the field: Fresh fist-sized (>250 g) intrusive and extrusive volcanic samples were collected from outcrops near joints. To avoid isotopic shifts caused by weathering, samples were cleaned of weathered rind by chiseling 2 to 3 cm from the edges.
2. In the laboratory: Samples were cut in half. Slabs and thin sections were prepared from one half. The other half was crushed in a jaw crusher. A split of 105 g was pulverized to less than 200 mesh. Of this, 100 g were used for X-ray and chemical analysis and 5 g prepared for whole-rock oxygen isotope analysis.
3. Initially carbonate was removed from the powders prepared for isotopic analysis in cases where the powder fizzed when exposed to dilute HCl. This was done using sodium acetate. It was later found that treated and untreated whole-rock samples only differed by ~0.1 per mil, so the carbonate removal procedure was stopped.
4. Eighty-three percent (489 of 588) of the oxygen isotope analyses were made by Krueger Enterprises Inc. of Cambridge, Massachusetts. Ninety-nine analyses were done by Sam Savin at Case Western Reserve University. The procedure in both laboratories was basically standard (Clayton and Mayeda, 1963). Bromine pentafluoride was reacted at 400° to 690°C (depending on mineralogy) to extract O_2 gas from the silicate samples. Samples from 1987 were analyzed by Krueger using a procedure wherein oxygen liberated from the rock was analyzed directly by the mass spectrometer, avoiding the normal hot carbon rod conversion of O_2 to CO_2.
5. All the isotope ratios are reported relative to SMOW referenced to NBS 28 = 9.6 per mil. Eight samples which were analyzed by both labs showed a difference of 0.12 ± 0.57 per mil, indicating that interlab variability is minor.

Oxygen Isotope Results

Statistical analysis

The mean of the $\delta^{18}O_r$ values from all 478 sites in the survey is 7.4 per mil with a variance of 4.0 and a standard deviation of 2.0 per mil. The $\delta^{18}O_r$ values for all sites, all samples, or all determinations are normally distributed. A histogram of all 588 determinations is shown in Figure 6.

The results of a nested analysis of variance (SAS Inst. Inc., 1985, chap. 24) are shown in Figure 7 top. The total variance of analyses from 1983 to 1985 (478 isotopic measurements from samples collected at 371 sites, including Beaty's 26 sites) is 3.8 per mil. The mean of the entire population is 7.5 per mil with

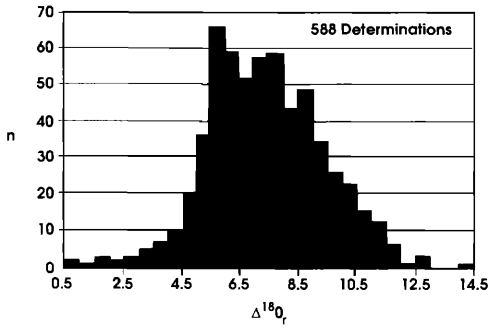

FIG. 6. Histogram of all $\delta^{18}O_r$ determinations reported in this study (see Appendix). The distribution is gaussian (Kolmogorov-Smirnov significance of 0.2, where <0.05 suggests nongaussian; skewness = 0.03; kurtosis = 0.30) and has a standard deviation of 2 per mil.

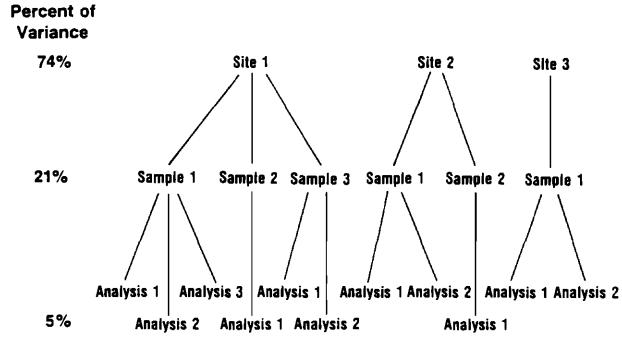

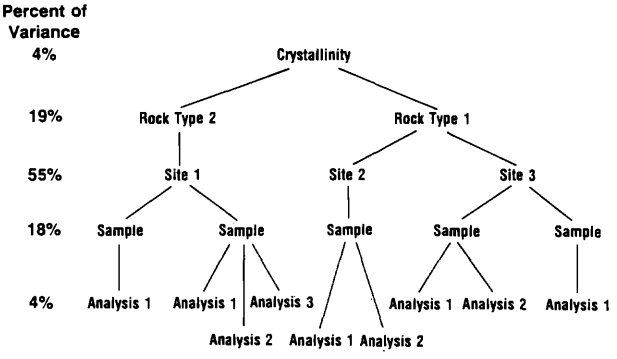

FIG. 7. Top. A nested analysis of variance of 478 oxygen isotope determinations from 371 sites shows about 74 percent of the isotopic variation is geographic. Bottom. Nested analysis of variance on 259 oxygen isotope determinations for which petrographic determinations of the original rock type are available shows that the variance associated with rock type is about the same as that associated with different samples at the same site.

a standard deviation of 1.9 per mil. The variance at the analysis level is 0.2 per mil and equivalent to a one sigma standard deviation of 0.4 per mil. This value agrees well with Krueger's laboratory data for many thousands of samples that indicates an analytical reproducibility for powdered silicate samples of $\sim \pm 0.5$ per mil. The variance at the analysis level plus the variance due to sampling different locations of the same local outcrop is 1.0 per mil which is equivalent to a standard deviation of 1 per mil. The nested variance analysis thus indicates that any variation greater than ± 1 per mil should be ascribed to geographic variation that has potential significance for mapping the paleohydrothermal system. Seventy-four percent of the total variance is at the site (geographic location) level. The geographic variance will be manifest in undulations in a 2 per mil interpretive band drawn around profiles of the isotopic data.

Two hundred thin sections were examined petrographically by Margaret S. Woyski (California State University at Fullerton) in order to determine the original rock type. These and a number of other samples were given a rock type code from 0.5 to 3.0 depending on lithology, and a crystallinity code distinguishing intrusive (1.0) from extrusive (0.0) samples. Porphyritic samples were given intermediate crystallinity values. The relationships between the numerical codes and commonly used rock names are given in Table 1.

Figure 7 bottom shows the results of a nested analysis of variance of 259 oxygen isotope determinations that includes rock type and crystallinity code as well as site, sample, and analysis. Very little of the total variance is associated with crystallinity. This is partly due to the fact that samples were collected to avoid diorite and gabbro intrusions that could be postmineralization (see later discussion). The crystalline population is therefore weighted with synmineralization intrusions such as the Flavrian pluton that equilibrated with the hydrothermal fluids, as did the adjacent extrusions. The variance associated with rock type is about the same as that associated with sampling an outcrop. Geographic location remains the single most important contributor to variations in whole-rock oxygen isotope signature.

TABLE 1. Rock Type and Crystallinity Codes Assigned to Rock Types in the Noranda Sample Suite

	Crystallinity	
Rock type	0.0	1.0
3.0	Rhyolite (V2)	Granite
2.5	Dacite (V4)	Tonalite
2.0	Andesite (V6)	Diorite
1.5	Basaltic andesite	
1.0	Basalt (V7)	Gabbro
0.5	Mafic basalt	

V2-V6 are the codes given on maps of the Ministry of Natural Resources of Quebec

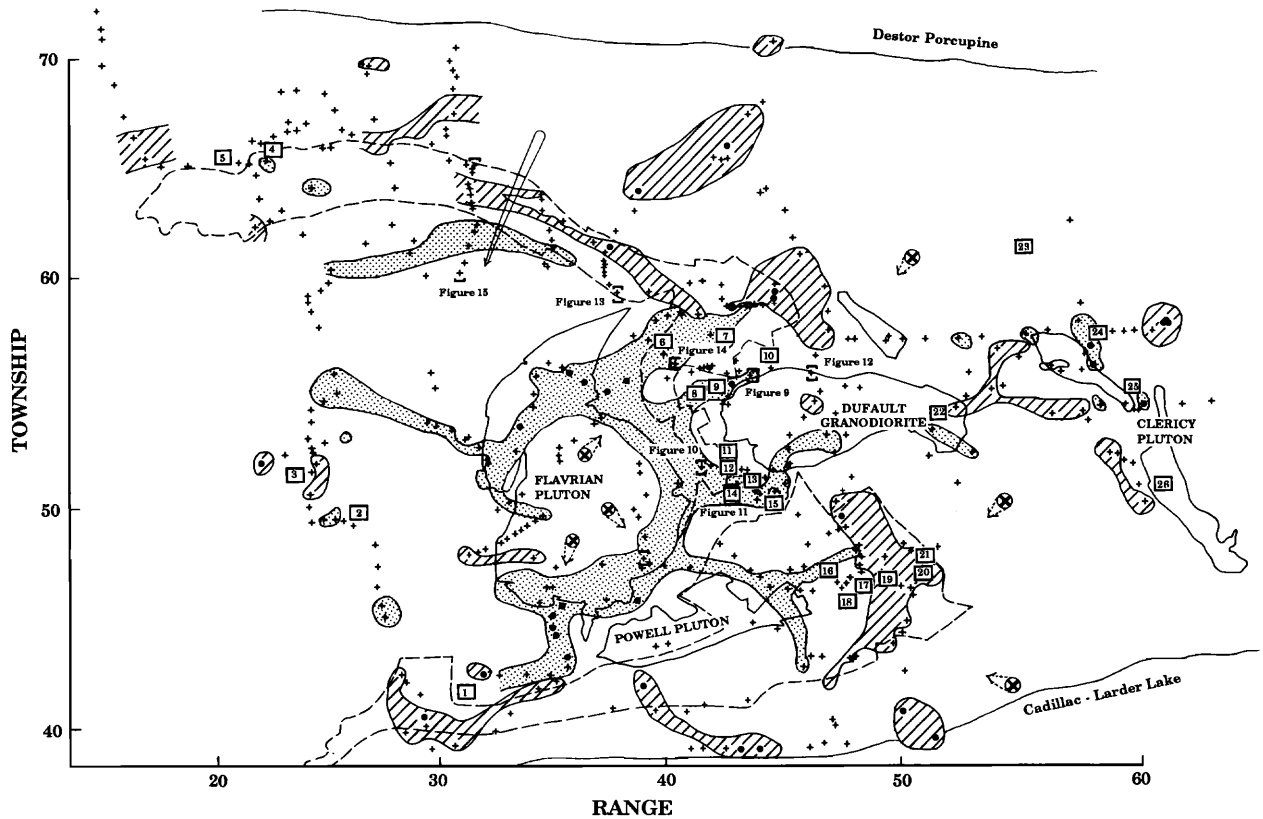

FIG. 8. Location of sites (+'s) in the Noranda area whose $\delta^{18}O_r$ values have been used in this study (see Appendix). The sites include those from which samples were collected in this study, plus 26 sites from Beaty (1980). Site $\delta^{18}O_r$ values were determined by first averaging all replicate analyses of samples collected from an outcrop and then averaging all outcrop samples. Contours are drawn around all $\delta^{18}O_r$ site values $\geq$ 9 per mil (1.5 standard deviations above the mean). These $^{18}O_r$-enriched areas are cross hatched. Contours are drawn around all $\delta^{18}O_r$ site values $\leq$ 6 per mil (1.5 standard deviations below the mean). These $^{18}O_r$-depleted areas are stippled. Sites with $\delta^{18}O_r > 11$ or <4 per mil are indicated with solid dots rather than +'s. The Mine sequence rhyolites from Quebec Ministry of Natural Resources 1:50,000-scale geologic maps and Hubert et al's. (1984) interpretation are outlined with a dashed line. The outlines of the principal plutons are indicated by solid lines. These features provide geologic reference. Possible areas of fluid recharge are indicated by arrows. Portions of the arrows below the present surface are dashed; the feathered end of the arrow is indicated by an "x." As discussed in the text the recharge across the Mine sequence volcanics near the label for Figure 15 may in fact have been the reverse of that shown (e.g., weak discharge along the edge of a northwestern extension of the Flavrian pluton). Locations of the principal massive sulfide deposits are indicated by numbers: 1 = Aldermac, 2 = Four Corners, 3 = Montbray, 4 = Fabie Bay, 5 = Magusi River, 6 = Ansil, 7 = Vauze, 8 = Old Waite, 9 = East Waite, 10 = Norbec, 11 = Amulet E, 12 = Amulet, 13 = Amulet A, 14 = Corbet, 15 = Amulet D and Millenbach, 16 = Joliet, 17 = Quemont, 18 = Horne, 19 = Donalda (Au), 20 = Delbridge, 21 = Deldona, 22 = Les Mines Gallen, 23 = Mobrun, 24 = Windfall, 25 = Harvie, 26 = Mine d'Etaine. The sites or profiles illustrated in Figures 9 to 15 are indicated and labeled with the "Figure" reference.

Isotopic pattern

The regional isotopic pattern can be shown in a number of fashions, computer and otherwise. One of the most informative was found to be simply outlining the regions where $\delta^{18}O_r \geq 9$ per mil and $\delta^{18}O_r \geq 6$ per mil. This is done in Figure 8. To construct this figure, replicate isotopic determinations of each sample were first averaged and then all site samples were averaged. The resulting site $\delta^{18}O_r$ values were then plotted at a 1:50,000 scale and contours constructed such that no sites with $\delta^{18}O_r$ values outside the ranges indicated fall inside the contours. The sites are indicated by "+." Those sites within the contour with $\delta^{18}O_r \geq 11$ per mil and ≤ 4 per mil are identified by solid dots.

Geologic reference is provided in Figure 8 by the outlines of the principal intrusive bodies and by the outline of the rhyolitic units of the Mine sequence volcanics. The latter was taken from the 1:50,000

geologic syntheses of the Ministry of Energy and Resources, Quebec (V2 units), following the general interpretation of Hubert et al. (1984). The Mine sequence identification is considered uncertain mainly in the northwest (from the Vauze to the Fabie Bay deposits) and in the area around the Horne and Delbridge deposits. Kerr and Gibson (1993), for example, place the Delbridge and Deldona deposits in cycle IV volcanics (not the cycle III, Mine sequence volcanics).

The most obvious feature of the alteration is the annulus of $\delta^{18}O_r \leq 6$ per mil that nearly surrounds the Flavrian pluton. The ^{18}O depletion, which includes the host volcanics as well as the intrusion, nearly rings the pluton and is open only to the west. Although most of the interior parts of the Flavrian are between 6 and 7 per mil, there are some sites that are strongly enriched in ^{18}O (8–>9‰). Six isotopically light fingers radiate from the ring. Four of these point up section toward massive sulfide deposits to the east. Farther to the east, and also to the north and south near the breaks, is a ~10-km-wide band of less continuous but equally intense positive $\delta^{18}O_r$ anomalies. The entire pattern, consisting of the light edge alteration and the heavy surrounding alteration, is ~30 km in diameter.

The Clericy intrusion shows a similar annular pattern of light isotopic alteration surrounded by $^{18}O_r$ enrichment. The scale of the alteration is considerably smaller, however (~10 km diam). No pattern of isotopic alteration is associated with the Powell and the Dufault intrusions.

There are relatively few anomalies (light or heavy) to the west of the Flavrian. There are a few patches of $^{18}O_r$ enrichment associated with the Montbray deposit and one light finger that possibly extends from the Flavrian. An east-west coherent band of ^{18}O depletion lies to the northwest of the Flavrian, just under and cutting slightly into the westward extension of the Mine sequence rhyolites.

The pattern of alteration shown in Figure 8 is consistent with the two other isotopic studies reported in this issue. Paradis et al. (1993) show a very regular increase in $^{18}O_r$ across the Mine sequence volcanics northeast of the Vauze massive sulfide deposit and also document a decrease to very depleted $^{18}O_r$ toward the Flavrian pluton. Hoy (1993) documents an up-section increase in the $\delta^{18}O_r$ values in the rocks surrounding massive sulfide deposits from the Corbet to the Ansil deposits, the Amulet A, and then the Norbec. He also shows that the alteration around the Horne mine is isotopically heavy. These same alteration trends are evident in Figure 8.

Although there are exceptions, the overall coherency of the alteration is remarkable. The coherency, and also the utility of the 2 per mil interpretive band suggested by the statistical analysis, can best be appreciated by examining parts of Figure 8 in detail. This is done for specific sites or profiles in Figures 9 to 15. The locations of these sites or profiles are indicated in Figure 8.

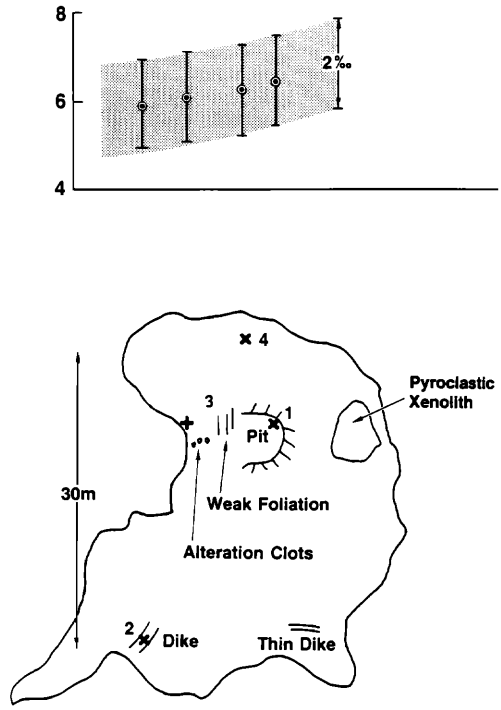

FIG. 9. Samples collected from site 1001, a small gabbro outcrop northeast of the Dufault granodiorite are indicated on a plan map of the outcrop. The $\delta^{18}O_r$ determinations are plotted as a function of latitude above the map. All the analyses fall within the analysis plus site error band of 2 per mil, visually confirming the nested variance analysis that suggests that isotopic variations associated with geographic location should lie outside this band. The outcrop is located in Figure 8.

Figures 9 to 11 show that isotopic variations at individual sites fall within the statistically indicated 2 per mil regional interpretive band. The gabbro outcrop northeast of the Dufault granodiorite in Figure 9, for example, shows a smoothly varying isotopic composition. A small basaltic dike cutting the outcrop is isotopically concordant. Similarly the wide range of volcanic lithologies and intrusions encountered within a 45- by 135-m part of the McDougal Dispina fault near the Corbet mine east of the Flavrian pluton (Fig. 10) all have isotopic compositions falling within the 2 per mil band. The volcanics encountered along the main Corbet haulage tunnel fall within the 2 per mil band, with the exception of a sample of the Lewis exhalite. On an outcrop scale the igneous rocks thus appear to have been homogenized by the hydrothermal circulation to within ±1 per mil.

This interpretation is supported by the fact that plutons which intruded the volcanic pile after most of the massive sulfide deposits had formed offset the 2

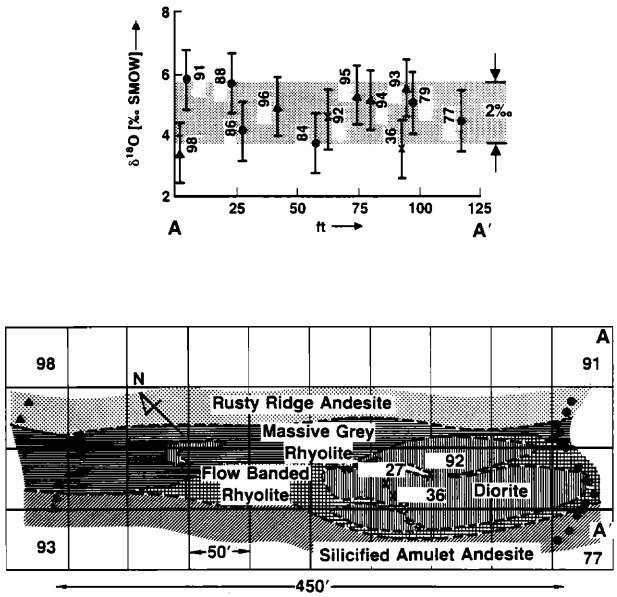

FIG. 10. Samples collected from site 1077. This site is a part of the McDougall-Despina fault near the Corbet mine that has been intruded by a variety of rhyolites and diorites. The sketch map was prepared from a field layout by Setterfield (1984). All the samples collected are indicated in the plan map, but only those isotopically analyzed are plotted on the $\delta^{18}O_r$ diagram. All samples lie within the 2 per mil analysis plus site error band and are depleted in ^{18}O compared to unaltered volcanics suggesting that all intruded prior to much of the hydrothermal circulation driven by the Flavrian pluton and that all have been shifted a similar amount by the hydrothermal circulation. The site is located in Figure 8.

per mil interpretive band. The northern edge of the Dufault granodiorite is 3 per mil heavier than adjacent basalts (Fig. 12). Similarly, a diorite unit that crosscuts the Mine sequence volcanics near where the Hunter Creek fault cuts the Flavrian Lake pluton (Fig. 13) is depleted in $^{18}O_r$ by ~4 per mil relative to adjacent rhyolites. These offsets are too large to attribute to isotopic differences in the magmas, and therefore, suggest that the units intruded after the Mine sequence volcanics were isotopically altered by the hydrothermal circulation, and that there was relatively little later hydrothermal circulation and alteration. This was certainly the case for the Dufault granodiorite which metamorphoses the feeder pipes of the Amulet deposits and therefore must be postmineralization. In general, it may be possible to identify postmineralization intrusion from their oxygen isotope mismatch with their environment.

Figures 14 and 15 show that comparatively large amplitude and locally coherent regional variations in oxygen isotope signature are superimposed on the 2 per mil-wide band. Figure 14 is an east-west profile cutting across the Mine sequence volcanics from the Ansil toward the Norbec deposit. It shows a smooth undulation with no offsets across volcanic units. Pillow cores are isotopically similar to pillow margins, within ±1 per mil.

The profile in Figure 15 is particularly interesting because it crosses the Mine sequence volcanics to the northwest of the Flavrian pluton in a 20-km gap between the Fabie Bay and Ansil deposits. The Mine sequence dips to the north at ~60° to 80° at this location (Hubert et al., 1984) so that the profile is nearly a section of the volcanic stratigraphy. This is the location where fluids, circulated by heat from the Flavrian granite and discharged at known deposit sites, would logically recharge. There is a discontinuity at the top in a position that could have been the paleosurface during the most active interval of hydrothermal circulation and massive sulfide deposition. Uncertainties in extrapolating the individual units of the Mine sequence volcanics make the exact location of the ore horizon uncertain. Just below the hypothesized ore horizon the volcanics are enriched in ^{18}O by ~3.5 per mil. Three kilometers down section along the traverse the basalts and andesites are depleted in ^{18}O by ~2.5 per mil. Farther down section they are relatively unshifted in ^{18}O. The profile thus shows a very coherent variation through a 5-km section that corresponds closely to the recharge profile observed in the ophiolites in Oman (Gregory and Taylor, 1981) and shown by the models (e.g., the right-hand side of Fig. 5d). The isotopic pattern shown in Figure 15 could thus have been caused by the flow of seawater into the section, with initial equilibration producing the ^{18}O enrichment in the volcanics, and by deeper circulation up the geothermal gradient producing the ^{18}O depletion in the volcanics.

However, as discussed below, there is a good correlation between $\delta^{18}O_r$ values and wt percent SiO_2, and no correlation between $\delta^{18}O_r$ values and boron along the profile, suggesting that the isotopic alteration was caused by weak hydrothermal discharge. Gravity and magnetic patterns in the area allow the interpretation that the Flavrian pluton extends north so that its edge could lie under much of the east-west-trending, ^{18}O-depleted band transected by the intake profile shown in Figure 15. If this is the case, essentially all of the light < 5 per mil alteration shown in Figure 8 is related to upward fluid flow along the edges of intrusive bodies.

Discussion

The most striking aspect of the isotopic alteration is the coherency, breadth, and lightness of isotopic alteration at the edges of the Flavrian Lake pluton and the light isotopic fingers that protrude up section into the Mine sequence volcanics and toward most of the massive sulfide deposits at Noranda. There is, of course, some latitude in how the envelopes are drawn where data are sparse. The contouring in these areas was guided by the patterns expected from the

model computations. Where discretion has been exercised is apparent from the site locations (+'s).

The Flavrian pluton is clearly more intensely and extensively depleted in $^{18}O_r$ than the other intrusions in the area. All of the 10 traverses across the margins of the Flavrian show isotopic alteration < 6 per mil. All but two of these traverses have coherent <6 per mil alteration over distances greater than 2 km. Twelve of the 64 sites with $\delta^{18}O_r < 6$ per mil have $\delta^{18}O_r < 4$ per mil. By contrast, only two of the four traverses across the Dufault granodiorite have sites with $\delta^{18}O_r < 6$ per mil and none have values < 4 per mil. Because isotopic alteration from the Flavrian pluton continues smoothly into the Dufault granodiorite, the alteration in and near the Dufault appears to be related to the Flavrian hydrothermal system rather than to any separate hydrothermal circulation driven by the Dufault intrusion. In other words the Flavrian alteration appears to be superimposed on the Dufault. This is not true for the Clericy intrusion. All of the three traverses across the Clericy show isotopic alteration < 6 per mil. Three sites have $\delta^{18}O_r <$ 4 per mil. The light alteration is near the northern part of the Clericy only and is surrounded by heavy alteration. The pattern of light and heavy alteration is similar to but clearly distinct from that of the Flavrian but is of much smaller scale (~10 km diam).

The intensity of $^{18}O_r$ depletion around pluton margins appears to correlate with the intensity of massive sulfide mineralization associated with the pluton. Massive sulfide mineralization at Noranda is almost entirely associated with the Flavrian pluton (Kerr and Gibson, 1993) which is also the most intensely $^{18}O_r$-depleted intrusion. The cycle III Mine sequence volcanics host 14 massive sulfide deposits. Three massive sulfide deposits are hosted in cycle IV volcanics, the Deldona, Delbridge, and Mine Gallen, but as discussed below, two of these appear (on the basis of the $^{18}O_r$ alteration pattern) to be associated with the Flavrian hydrothermal system. The Clericy intrusion (cycle V) has three associated massive sulfide deposits (the Mobrun, the Harvie, and Mine d'Etain). The Clericy deposits are generally located between the light margin alteration of the Clericy pluton and

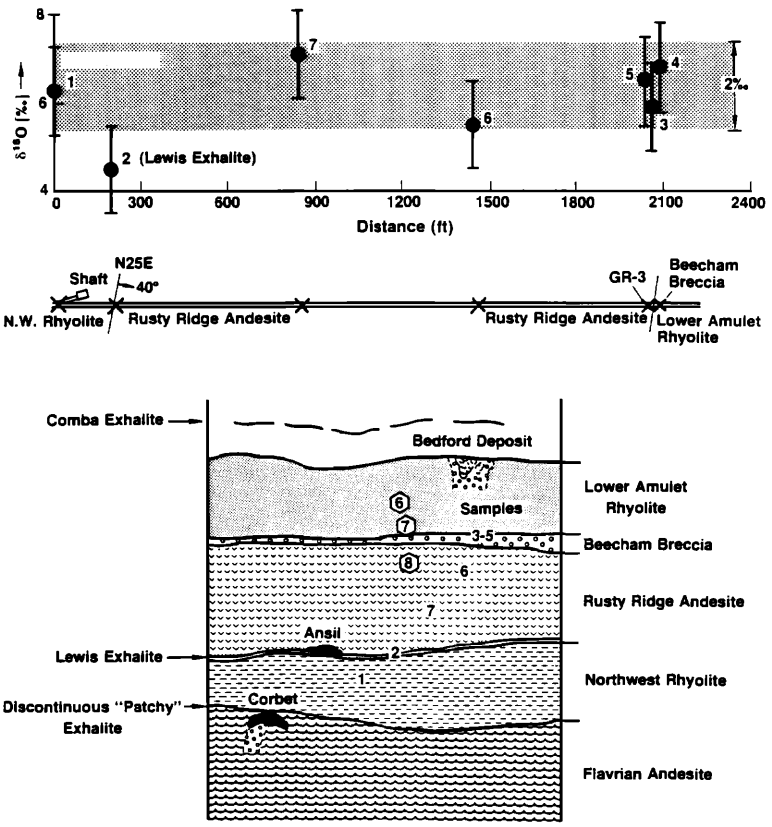

FIG. 11. Samples along the Corbet mine main haulage tunnel show little oxygen isotope variation over 2,100 ft. These subsurface samples are not included in the Appendix and have no site number assigned, but the Corbet mine is located in Figure 8. The samples are located on a geologic section prepared by Harold Gibson that was distributed as a mine tour map at the time the samples were collected.

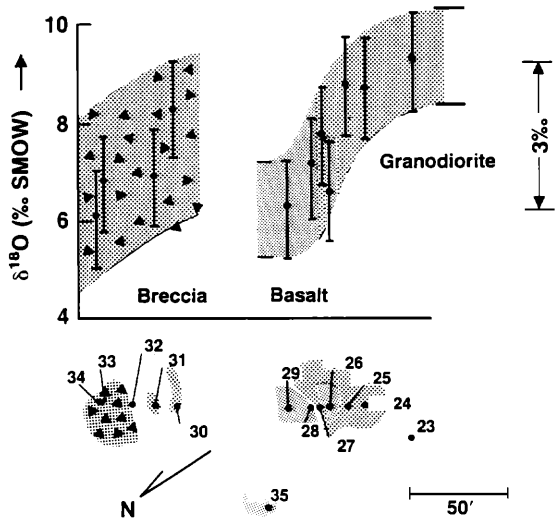

FIG. 12. Samples collected from site 1123, the northern margin of the Dufault granodiorite, are shown in a plan map sketch. The subset of the samples that was analyzed isotopically is plotted. There is a significant offset in isotopic composition of samples across the contact confirming that the Dufault intruded after most of the hydrothermal circulation driven by the Flavrian pluton was complete. The site is located in Figure 8.

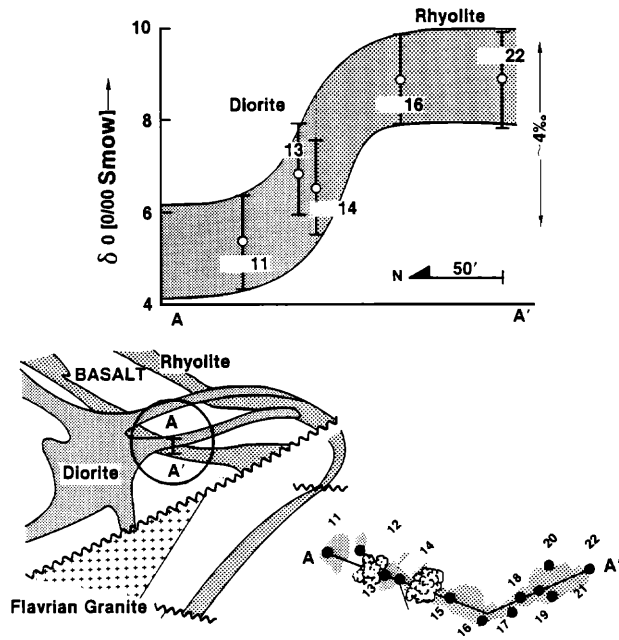

FIG. 13. Samples collected from site 1111, a short transect across a diorite dike that crosscuts the Mine sequence volcanics just north of the northern end of the Flavrian pluton, are shown in plan. The subset of these samples that was analyzed isotopically is plotted. The ~4 per mil isotopic offset across the diorite contact suggests that the diorite intruded after most of the Flavrian hydrothermal circulation was completed.

surrounding heavy $^{18}O_r$ alteration, as are most of the massive sulfide deposits associated with the Flavrian pluton.

The Deldona (Zn, Ag, Au) and Delbridge (Zn, Cu, Ag, Au) deposits lie at the top of a heavy $^{18}O_r$ mushroom-shaped cap that is draped over one of the fingers of light alteration extending from the Flavrian margin to the Horne, Quemont, and Joliet massive sulfide deposits, the largest in the Noranda camp. The permeable plumbing system which must have been associated with the Horne and Quemont deposits makes this a likely location for weak hydrothermal circulation to continue into cycle IV. The Deldona and Delbridge deposits thus appear, on the basis of oxygen isotope alteration, to be associated with the final stages of the Flavrian hydrothermal event rather than with a cycle IV hydrothermal system.

The isotopic alteration is compatible with the model calculations presented in Figure 5. The light alteration around the intrusion margins is almost certainly caused by the up-temperature gradient migration of fluids that are heated and circulated along them. The annular pattern suggests that the heat source lay beneath the felsic cap and that the most permeable channels were along the margins of the intrusion. The light isotopic fingers extending up section from the Flavrian probably correspond to the light prongs in Figure 5c that extend upward from the model intrusion margin. Particularly the heavy alteration draped over the top of the largest massive sulfide deposits, the Horne and the Quemont, may correspond to the heavy fugitive anomaly that migrates with the thermal anomaly in the calculations.

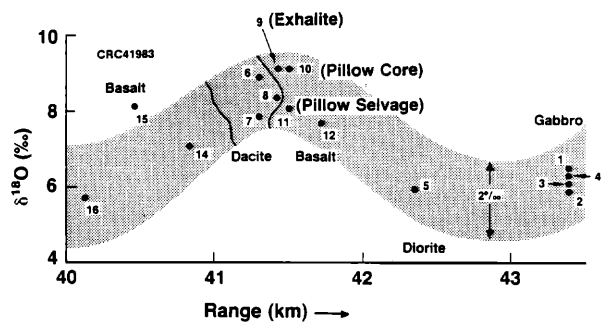

FIG. 14. The $\delta^{18}O_r$ values of samples collected along a 3.5-km east-west profile across the Mine sequence volcanics from the Ansil to Norbec deposits that passes through the main contact exhalite are plotted against the range coordinate. Rock type is indicated along the transect which runs as indicated from site 1001 through site 1016. Numbers in the diagram correspond to the last one or two digits in the sample number with the exception of the first four samples which are all from site 1001 and are also plotted in Figure 9. The smooth isotopic undulation of the 2 per mil regional band illustrates the utility of this band for visualizing the regional isotopic variations that map a hydrothermal system. The transect is located in Figure 8.

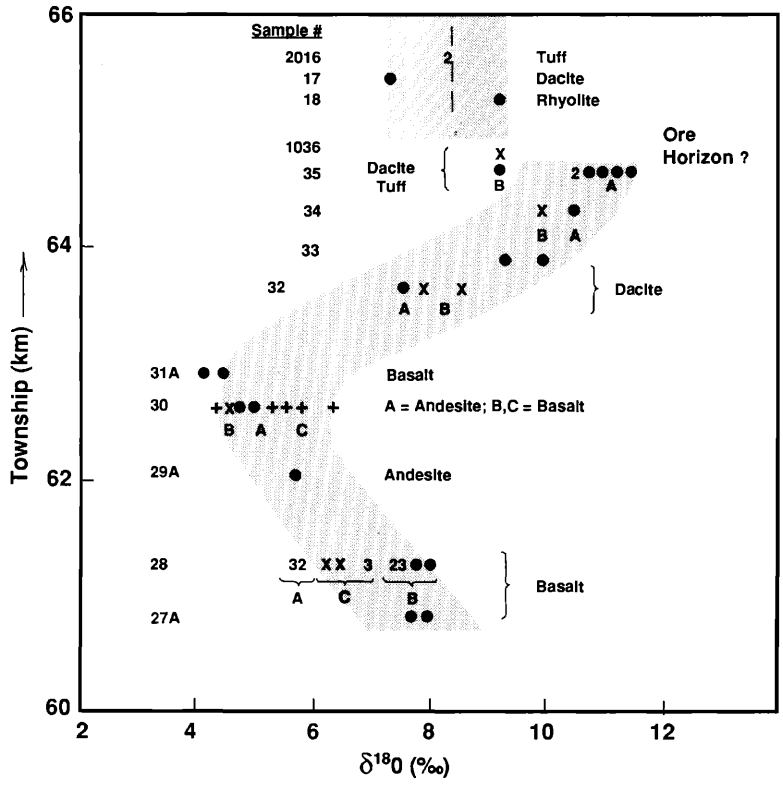

FIG. 15. The $\delta^{18}O_r$ values of samples collected along a traverse crossing the Mine sequence volcanics in a possible seawater recharge location between the Ansil and Fabie Bay deposits are plotted. The profile shows a smooth variation similar to that found in a cross section of the Samail Ophiolite and calculated in the right-hand part of Figure 5d. The strata are dipping ~70° N so the profile provides a section through the volcanic pile. The profile can be interpreted to terminate (e.g., return to unshifted isotopic values) at a position that could correspond to the ore horizon. The alteration could be caused by the inflow of seawater at the time of mineralization. Alternatively, as discussed in the text, the light and overlying heavy bands could have been produced by weak, diffuse discharge along the boundary of a possible eastern extension of the Flavrian pluton. Samples are from 2000 and 1000 series sites. At each site, samples from different locations on the outcrop are lettered (A, B, C). Analyses of a single sample are given a distinctive symbol (●, x, +). Where analyses overlap on the plot numbers are used to indicate the number of overlapping analyses. The traverse is located in Figure 8.

This crescent or (in three dimensions) mushroom cap-shaped anomaly is best developed in Figure 5b because in the model calculations it is destroyed (pushed through to the surface) as hydrothermal discharge continues. In an accumulating volcanic pile it would not be destroyed but would instead migrate higher in the section.

The main uncertainty with this interpretation is that the heavy cap above the Horne that incorporates the Delbridge and Deldona deposits could have been produced by a possible late pulse of gold-rich fluids expelled during tectonic compression, not during the waning stages of the Flavrian hydrothermal system. The permeable Horne plumbing system would have channeled this hydrothermal pulse just as it did the Flavrian circulation. The presence of the Donalda (Au, Ag) deposit between the Horne and the Delbridge massive sulfide deposits and the gold-rich nature of the Horne reinforces this possibility. Heavy $^{18}O_r$ alteration associated with a pulse of gold mineralization is quite likely both above the Horne and along the breaks.

However, even if some of the heavy isotopic alteration was produced by a late, gold-depositing hydrothermal pulse, the location of the Delbridge and Deldona deposits still suggests an association with the Flavrian hydrothermal system. From a chemical perspective it is also most likely that a convecting fluid of seawater salinity driven by the Flavrian persisted long enough to form these massive sulfide deposits and that a later pulse of low-salinity fluid deposited the gold (e.g., Cathles, 1986). Thus the most likely picture that emerges from the isotopic pattern and modeling is that a very large scale hydrothermal system was driven over a substantial period of time by the underlying, probably mafic, counterparts of the

Flavrian pluton. This hydrothermal system was waning at the time the Dufault granodiorite intruded, but was still sufficiently active to produce the Deldona and Delbridge massive sulfide deposits within the cycle IV volcanic section.

Discharge appears to have been fairly continuous along the eastern margin of the Flavrian. Recharge through the present surface probably occurred in the south along what is now the Cadillac-Larder Lake break, through the top of the Mine sequence volcanics where it is buried east of the deposits, and perhaps in the north in the gap between massive sulfide deposits where samples for the intake profile shown in Figure 15 were collected. There was probably also recharge into the central parts of the Flavrian pluton; this could explain the heavier interior alteration and help define the annular ring of light alteration at the margin. An annular pattern of discharge with recharge over the central parts of a pluton is expected for large plutons (Cathles, 1978) and would be further promoted if a deep mafic body were the heat source and the interior parts of the Flavrian cap less permeable than the margins and adjacent volcanics. Possible recharge areas are indicated by arrows in Figure 8.

If the sequences in general plunge east as indicated in Figure 2, the finger pointing west on the west side of the Flavrian is an anomaly. It could reflect hydrothermal circulation associated with the very early stages of development, down section, of the Flavrian intrusive center. Or it could indicate unrecognized stratigraphic complexities. As one moves up section to the east, the isotopic alteration records the increase and finally decrease in hydrothermal circulation. The comparatively small hydrothermal system associated with the Clericy pluton developed later, distinct from the Flavrian system.

If the Flavrian hydrothermal system did overprint the cycle IV Dufault granodiorite and its associated extrusions, as suggested by the heavy $^{18}O_r$ anomaly near the Delbridge and Deldona deposits, the hydrothermal system was remarkably long-lived as well as of remarkable spatial scale. Certainly the hydrothermal system seems to have been active for the entire period of time the Mine sequence volcanics were erupting. The hydrothermal system thus probably lasted for ~10 m.y., from the solidification of the felsic Flavrian cap at 2700 Ma to the solidification of the Dufault granodiorite at 2690 Ma. Magma replenishment would be required to sustain a hydrothermal system for this long (e.g., Cathles, 1981; Cathles et al., 1983). The scale of the alteration pattern suggests that fluids circulated deep into the volcanic pile. Hydrothermal circulation cells tend to be approximately equidimensional. The 10- to 15-km separation of likely recharge areas from the edges of the Flavrian suggests that convection occurred through the full 8- to 13-km-thick greenstone section of the crust.

It would be useful to have a chemical indicator of flow direction to verify the interpretations given above. In particular, it would be useful if some chemical alteration could distinguish heavy isotopic alteration caused by seawater intake from heavy alteration caused by down-temperature gradient flow. Sr isotopes cannot be used to identify seawater recharge in the Archean as they were in the Oman ophiolite, since prior to ~2.5 Ga strontium isotope ratios in ocean water were similar to those of the mantle and in mantle-derived volcanic rocks (Veizer and Compston, 1976). Also, since whole-rock oxygen isotope analysis is expensive, it would be preferable if less expensive kinds of chemical analysis could provide the same information as the isotopic determinations. One hundred and twenty-nine of the samples collected in 1983 were analyzed chemically to address these questions, unfortunately with negative results.

These samples were analyzed by X-ray fluorescence by Probatech Inc. of Naughton, Ontario, for SiO_2, TiO_2, Fe_2O_3, Al_2O_3, MnO, MgO, CaO, Na_2O, K_2O, and P_2O_5. The degree of alteration was determined by Probatech using the approach of Beswick and Soucie (1978). This method determines the discrepancy between the chemistry of a sample and the chemistry expected from the differentiation trend of the sample suite, assuming Al_2O_3 is immobile. Both the whole-rock chemistry and the percent change in the oxides that was caused by metasomatic alteration are reported. The analytical data are available from the author upon request.

The chemical changes between unaltered and altered rock determined by Beswick and Soucie (1978) show no obvious spatial patterns. When the 129 analyses are regressed against $\delta^{18}O_r$, ΔTiO_2 correlates best with $\delta^{18}O_r$, but the magnitude of the correlation coefficient is low (−0.505). The next highest correlation is with ΔFe_2O_3 at −0.317. Present rock chemistry correlates as well or better. The correlation coefficients between $\delta^{18}O_r$ and wt percent K_2O, TiO_2, Al_2O_3, and SiO_2 are 0.57, −0.51, 0.47, and −0.42, respectively. Along specific traverses the correlations can be much better. For example, the correlation coefficients between $\delta^{18}O_r$ and wt percent TiO_2, SiO_2, Fe_2O_3, and Al_2O_3 are −0.89, 0.85, −0.80, and −0.78, respectively, for 13 analyses along the intake profile shown in Figure 15. These data agree with the results of MacLean and Hoy (1991) and Barrett and MacLean (1991) who find good correlations between SiO_2 and $\delta^{18}O_r$ for samples near the Horne and Inmont massive sulfide lenses. Apparently the correlation between SiO_2 and other rock components deteriorates as the size of the area sampled increases.

Thirty-two pulps were submitted for boron analysis to X-Ray Assay Laboratories, Don Mills, Ontario. The samples were collected mostly along the profile shown in Figure 15 to see if boron from seawater was added to the rock in recharge areas. No correlation

was found between $\delta^{18}O_r$ and B along the profile, or for all 32 samples. Along the profile the correlation coefficient was 0.12; it is lower for the full 32 samples.

There thus seems to be no general correlation between oxygen isotope alteration and chemical alteration. For a large number of samples from broadly distributed sites there seems to be no simple way to predict the $\delta^{18}O_r$ value of a sample from its whole-rock chemistry, and we could find no chemical indication of seawater recharge (flow direction). Expressing chemical changes relative to the unaltered rock type using the methods of MacLean (1990) might produce better chemical correlations with $\delta^{18}O_r$. The lack of Zr analyses precludes using this method in the present study.

Mineralogic changes may also be a more promising proxy for oxygen isotope analysis as discussed, for example, by Taylor and South (1985), Schiffman and Smith (1988), Hoy (1993), and Paradis et al. (1993). Goldie (1979) has investigated the metamorphic and metasomatic alteration of the Flavrian and Powell plutons. There is a coherent distribution of isograds around the Flavrian and an indication that the edges of the pluton were most altered (e.g., the mineralogic assemblages at the Flavrian edges have the highest metamorphic temperatures and the greatest X_{CO_2}). The distribution of hornblende-bearing rock noted by Goldie is nearly coincident with the annulus of $\delta^{18}O_r < 6$ per mil shown in Figure 8. Both the $\delta^{18}O_r$ alteration and the high metamorphic temperatures suggest a deeper heat source, with thermal plumes flowing upward around the edges of the Flavrian pluton.

Exploration Implications of the Oxygen Isotope Survey at Noranda

Intense light oxygen isotope alteration at the edges of an intrusion appears to have exploration significance. The only way the margins of an intrusion, comprising both the intrusion itself and the adjacent host rocks, can be depleted in ^{18}O is for the intrusion to have circulated large amounts of water. Such intrusions can produce massive sulfide deposits where the hydrothermal fluids discharged in a focused fashion onto the sea floor. Massive sulfide exploration should be concentrated up section from intrusions, the edges and immediate host rock of which are depleted in ^{18}O. Light ^{18}O fingers pointing up section from the margins of an intrusion such as the Flavrian may mark flow channels and point to areas of concentrated discharge and massive sulfide mineralization. Fingers appear to point to nearly all the massive sulfide deposits associated with the Flavrian hydrothermal system. These observations have exploration implications in the Noranda camp and in general.

Regarding first the implications for the Noranda camp: the stratigraphy surrounding the Flavrian pluton generally dips and youngs to the east. The only major exception is the Dufresnoy tholeiite sequence which occupies a syncline to the northeast of the Flavrian. The area to the west of the Flavrian is mapped as entirely down section of the Flavrian by Hubert (1984). If this is indeed the case (the one light isotopic finger pointing to the west might warrant a reexamination of this stratigraphic interpretation), the Mine sequence volcanics and their extension to the east and north of the Flavrian are the most prospective strata for massive sulfide exploration. The area west of the Flavrian has limited exploration potential because it lies down section of the Flavrian heat source and because there is no isotopic or geologic indication of a major underlying heat source (intrusion). The Fabie Bay and Magusi River massive sulfide deposits were possibly produced by hydrothermal circulation driven by a small pluton (shown on some maps) to the west and down section of these deposits.

The lack of an ^{18}O-depleted halo around the Dufault pluton suggests that the area up section of the Dufault has low potential for hosting significant massive sulfide mineralization. It is interesting that the Dufault has a significant metamorphic halo (indicating cooling was not assisted by convective circulation; Goldie, 1979; Jolly, 1980) and the Flavrian does not. The Clericy intrusion may have exploration potential, because it shows significant ^{18}O depletion and has three nearby massive sulfide deposits, but it is a small intrusion compared to the Flavrian and has an isotope pattern one-third as large, so its potential for mineralization is not as big as that of the Flavrian.

The most important general implication of the study is that intrusions are prospective up section for massive sulfide deposits in proportion to their size and to the degree of ^{18}O depletion of their margins. Based on these observations at Noranda, the margins of intrusions in terrain that is permissive of massive sulfide mineralization, both in terms of geology and land availability, can be screened by sampling the margins of each intrusion with about five traverses of 5-km length. Samples should be collected every ~0.5 km along each traverse (for an average of 10 samples per traverse, or ~50 samples/intrusion). Exploration efforts should be focused up section from these intrusions. Exploration might be further focused where ^{18}O-depleted fingers project up section, especially if those fingers point toward an ^{18}O-enriched mushroom cap which indicates that hydrothermal activity persisted for a prolonged period of time in a particularly permeable plumbing. Massive sulfide deposits such as Horne and Quemont should be sought at the end of the ^{18}O-depleted finger and beneath the ^{18}O-enriched cap.

Exploration applications should be made of the concept that $^{18}O_r$-depleted intrusive margins indicate high massive sulfide exploration potential up section.

Such applications need not await the results of further research.

Summary and Recommendations for Further Research

The main conclusions indicated by the isotopic study reported in this paper are the following:

1. Five hundred and eighty-eight outcrop whole-rock ^{18}O analyses from 478 sites in a 35- by 50-km part of the Blake River syncline in the Noranda mining camp have a mean $\delta^{18}O_r$ value for intrusive and extrusive volcanics of 7.4 per mil. The variance of the sample population is 4 per mil.
2. A nested analysis of variance of 478 analyses of samples from the first 371 sites shows that 74 percent of the variance is associated with sample location and 26 percent with analytical error and outcrop variability. Oxygen isotope variations outside a 2 per mil band mostly reflect regional changes related to the hydrothermal circulation system that produced massive sulfide mineralization in the Noranda camp.
3. Outcrop studies and traverses across the area confirm the utility of a 2 per mil interpretive band (Figs. 9–15).
4. Offsets of the 2 per mil $\delta^{18}O_r$ interpretive band across the margins of dikes and intrusions indicate that they intruded after the hydrothermal circulation (Figs. 12 and 13).
5. Intrusions such as the Flavrian that drove significant hydrothermal circulation and produced massive sulfide deposits are distinguished mainly by having coherent $^{18}O_r$ depletion along their margins (Fig. 8).
6. Light marginal alteration projects up section toward sites of focused discharge and massive sulfide deposition. The largest massive sulfide deposits in the Noranda camp are at the end of a light isotopic finger and overlain, in the hanging wall, by an $^{18}O_r$-enriched mushroom cap (Fig. 8).
7. The hydrothermal system associated with the Flavrian pluton was of unusually large spatial scale (alteration 30 km in diam) and persisted for ~10 m.y. Fluid circulation was probably driven to ~8 to 13 km in depth.
8. A simple convective model (Figs. 3–5) can explain the massive sulfide-related oxygen isotope alteration at Noranda. The model explains both the isotopic composition of the vent fluids and the fluids that alter the edges of the intrusion as the natural evolution of the isotopic composition of the fluid from 0 per mil seawater to a depleted fluid at ~100°C, and then to a ~0 per mil fluid at the hot margins of the intrusion. The model can account for the observed progression of feeder pipe rock alteration from depleted values in the lower parts of the sequence to enriched at the top (Hoy, 1993). The model also accounts for the heavy isotopic alteration in the hanging wall, especially above late deposits.

The study suggests several avenues that should be pursued by further research:

1. The light isotopic fingers and mushroom caps around the margins of the Flavrian pluton shown in Figure 8 should be further defined. The objective should be to determine if light isotopic fingers point toward massive sulfide deposits and if large deposits have $^{18}O_r$-enriched caps up section.
2. The relation of isotopic alteration to gold mineralization along the breaks in the Noranda area should be investigated. Samples will need to be obtained largely from drill cores because the Destor-Porcupine and Cadillac-Larder Lake breaks are not well exposed. The objective should be to define any heavy oxygen isotope overprinting by late fluids responsible for gold mineralization. Overprinting could be in part responsible for the heavy $^{18}O_r$ of the Horne feeder pipe.
3. A way needs to be found to determine the direction of fluid circulation in Archean hydrothermal systems. In particular we need to be able to distinguish $^{18}O_r$ enrichment caused in the near surface by seawater recharge from the $^{18}O_r$ enrichment caused by diffuse (or limited) hydrothermal discharge.
4. Isotopic alteration on a regional scale needs to be mapped in detail in other massive sulfide camps. The Timmins area might be a good site and would have the added advantage of testing Beaty's (1980) brine hypothesis. The anomaly pattern at Noranda defined by 588 analyses is very different from the one Beaty (1980) identified on the basis of ~34 analyses from the Timmins area.
5. Although structural complications are minimized by the very large scale of the isotopic alteration, structural deformation should be taken into account when interpreting the regional distribution of $\delta^{18}O$ values resulting from pretectonic hydrothermal activity centered around intrusions.

Acknowledgments

I thank the Chevron Oil Field Research Company and Chevron Resources for supporting the project reported in this paper over a period of about five years, and for permission to publish the results. My first choice would have been for Chevron to use the results in an exploration program to find massive sulfide mineralization—the ultimate test of any concept and one I continue to believe is fully feasible. Unfortunately, curtailment of Chevron's mineral exploration efforts precludes this possibility. I also thank the Quebec Ministry of Energy and Resources for providing an infrastructure within which this research project could be carried out. Resident geologist Maurice Rive arranged mine tours and provided many helpful discussions that encouraged the research.

I thank Bill Hallager, Ted Glenn, Steve Uzmann, and Paulette Tylee for help in the field and for many interesting and instructive geological discussions. Dick Hutchinson suggested the Noranda area as a site for the field trial and spent three days orienting Hallager and me. Tom Ashbaugh isotopically analyzed some of the carbonates and Sam Savin, Paul Knauth, and Hal Krueger provided the remaining analyses and much good advice. Margaret Woyski carried out thin section studies that allowed initial rock-type determinations. Scott McKeag, Charlotte Kenison, and Jeff Parshley prepared the samples. Bill Hallager suggested the nested analysis of variance approach and Alan Trzcinko designed the Noranda data file and assisted in the statistical analysis. Steve Scott introduced me to the Noranda area. Dave Beaty's initial work got us started, and Ed Spooner and Tucker Barrie organized the symposium that provided the impetus for publication. The paper benefited greatly from the privilege of reading and citing the other papers in this volume, and from extremely thoughtful and detailed reviews by three *Economic Geology* referees.

REFERENCES

Barrett, T. J., and MacLean, W. H., 1991, Chemical, mass, and oxygen isotope changes during extreme hydrothermal alteration of an Archean rhyolite, Noranda, Quebec: ECON. GEOL., v. 86, p. 406–414.

Barriga, F. J. A. S., and Kerrich, R., 1984, Extreme ^{18}O-enriched volcanics and ^{18}O-evolved marine water, Aljustrel, Iberian pyrite belt: Transition from high to low Rayleigh number convective regimes: Geochim. et Cosmochim. Acta, v. 48, p. 1021–1031.

Beaty, D. W., 1980, The oxygen isotope geochemistry of the Abitibi greenstone belt: Unpub. Ph.D. thesis, California Inst. Technology, pt. 2, 463 p.

Beaty, D. W., and Taylor, H. P., 1982, Some petrologic and oxygen isotopic relationships in the Amulet mine, Noranda, Quebec, and their bearing on the origin of Archean massive sulfide deposits: ECON. GEOL., v. 77, p. 95–108.

Beaty, D. W., Taylor, H. P., and Coad, P. R., 1988, An oxygen isotope study of the Kidd Creek, Ontario, volcanogenic massive sulfide deposit, evidence for a high ^{18}O ore fluid: ECON. GEOL., v. 83, p. 1–17.

Beswick, A. E., and Soucie, G., 1978, A correction procedure for metasomatism in an Archean greenstone belt: Precambrian Research, v. 6, p. 235–248.

Bowers, T. S., and Taylor, H. P., 1985, An integrated chemical and stable-isotope model of the origin of midocean ridge hot spring systems: Jour. Geophys. Research, v. 90, p. 12583–12606.

Cathles, L. M., 1978, Hydrothermal constraints on the formation of kuroko deposits: Mining Geology, v. 28, p. 257–266.

—— 1981, Fluid flow and the genesis of hydrothermal ore deposits: ECON. GEOL. 75TH ANNIV. VOL., p. 424–457.

—— 1983, An analysis of the hydrothermal system responsible for massive sulfide deposition in the Hokuroku basin of Japan: ECON. GEOL. MON. 5, p. 439–487.

—— 1986, The geologic solubility of gold from 200–250°C, and its implications for gold-metal ratios in vein and stratiform deposits: Canadian Inst. Mining Metallurgy Spec. Vol. 38, p. 187–210.

Cathles, L. M., Guber, A. L., Lenagh, T. C., and Dudas, F. Ö., 1983, Kuroko-type massive sulfide deposits of Japan: Products of an aborted island-arc rift: ECON. GEOL. MON. 5, p. 96–114.

Clayton, R. N., and Mayeda, T. K., 1963, The use of bromine pentafluoride in extraction of oxygen from oxides and silicates for isotopic analysis: Geochim. et Cosmochim. Acta, v. 27, p. 43–52.

Cole, D. R., 1980, Mechanisms and rates of stable isotope exchange in hydrothermal rock-water systems: Unpub. Ph.D. thesis, University Park, Penn., Pennsylvania State Univ., 303 p.

Corfu, F., 1993, The evolution of the southern Abitibi greenstone belt in light of precise U-Pb geochronology: ECON. GEOL., v. 88, p. 1323–1340.

Costa, U. R., Barnett, R. L., and Kerrich, R., 1983, The Mattagami Lake mine Archean Zn-Cu sulfide deposit, Quebec: Hydrothermal coprecipitation of talc and sulfides in a sea floor brine pool—evidence from geochemistry, $^{18}O/^{16}O$, and mineral chemistry: ECON. GEOL., v. 78, p. 1144–1203.

Dimroth, E., Imreh, L., Rocheleau, M., and Goulet, N., 1982, Evolution of the south-central part of the Archean belt, Quebec. Part I: Stratigraphy and paleogeographic model: Canadian Jour. Earth Sci., v. 19, p. 1729–1758.

Forester, R. W., and Taylor, H. P., 1977, $^{18}O/^{16}O$, D/H, and $^{13}C/^{12}C$ studies of the Tertiary igneous complex of Skye, Scotland: Am. Jour. Sci., v. 277, p. 136–177.

Gelinas, L., and Ludden, J. N., 1984, Rhyolite volcanism and the geochemical evolution of an Archean central ring complex: The Blake River Group volcanics of the southern Abitibi belt, Superior province: Physics Earth Planet Interiors, v. 35, p. 77–88.

Gibson, H. L., and Watkinson, D. H., 1990, Volcanogenic massive sulfide deposits of the Noranda cauldron and shield volcano, Quebec: Canadian Inst. Mining Metallurgy Spec. Vol. 43, p. 119–132.

Goldie, R., 1979, Metamorphism of the Flavrian and Powell plutons, Noranda area, Quebec: Jour. Petrology, v. 20, p. 227–238.

Goodwin, A. M., 1977, Archean basin-craton complexes and growth of Precambrian shields: Canadian Jour. Earth Sci., v. 14, p. 2737–2759.

Goodwin, A. M., and Ridler, R. H., 1970, The Abitibi orogenic belt: Canadian Geol. Survey Paper 70-40, 30 p.

Green, A. G., Milkereit, B., Mayrand, L. J., Ludden, J. N., Hubert, C., Jackson, S. L., Sutcliffe, R. H., West, G. F., Verpaelst, P., and Simard, A., 1990, Deep structure of an Archaen greenstone terrane: Nature, v. 344, p. 327–330.

Green, G. R., Ohmoto, H., Date, J., and Takahashi, T., 1983, Whole-rock oxygen isotope distribution in the Fukazawa-Kosaka area, Hokuroku district, Japan, and its potential application to mineral exploration: ECON. GEOL. MON. 5, p. 395–511.

Gregory, T. T., and Taylor, H. P., 1981, An oxygen isotope profile in a section of Cretaceous oceanic crust, Samail Ophiolite, Oman: Evidence for $\delta^{18}O$ buffering of the oceans by deep (>5 km) seawater-hydrothermal circulation at mid-ocean ridges: Jour. Geophys. Research, v. 86, p. 2737–2755.

Hoffman, S. E., Wilson, M., and Stakes, D. S., 1986, Inferred oxygen isotope profile of Archean oceanic crust, Onverwacht Group, South Africa: Nature, v. 321, p. 55–58.

Hoy, L. D., 1993, Regional evolution of hydrothermal fluids in the Noranda district, Quebec: Evidence from $\delta^{18}O$ values from volcanogenic massive sulfide deposits: ECON. GEOL., v. 88, p. 1526–1541.

Hubert, C., Trudel, P., and Gelinas, L., 1984, Archean wrench fault tectonics and structural evolution of the Blake River Group, Abitibi belt, Quebec: Canadian Jour. Earth Sci., v. 21, p. 1024–1032.

James, D. E., 1981, The combined use of oxygen and radiogenic isotopes as indicators of crustal contamination: Ann. Rev. Earth Planet. Sci., v. 9, p. 311–344.

Jensen, L. S., and Langford, F. F., 1985, Geology and petrogenesis of the Archean Abitibi belt in the Kirkland Lake area, Ontario: Ontario Geol. Survey Misc. Paper 123, 130 p.

Jolly, W. T., 1980, Development and degradation of Archean lavas, Abitibi area, Canada, in light of major element geochemistry: Jour. Petrology, v. 21, p. 323–363.

Kalogeropoulos, S. I., and Scott, S. D., 1983, Mineralogy and geo-

chemistry of tuffaceous exhalites (tetsusekiei) of the Fukazawa mine, Hokuroku district, Japan: ECON. GEOL. MON. 5, p. 412–432.

Kerr, D. J., and Gibson, H. L., 1993, A comparison of the Horne volcanogenic massive sulfide deposit and intracauldron deposits of the Mine sequence, Noranda, Quebec: ECON. GEOL., v. 88, p. 1419–1442.

Larson, P. B., 1984, Geochemistry of the alteration pipe at the Bruce Cu-Zn volcanogenic massive sulfide deposit, Arizona: ECON. GEOL., v. 79, p. 1880–1896.

Letros, S., Strangway, D. W., Tasillo-Hirt, A. M., Geissman, J. W., and Jensen, L. S., 1983, Aeromagnetic interpretation of the Kirkland Lake-Larder Lake portion of the Abitibi greenstone belt, Ontario: Canadian Jour. Earth Sci., v. 20, p. 548–560.

MacLean, W. H., 1990, Mass change calculation in altered rock series: Mineralium Deposita, v. 25, p. 44–49.

MacLean, W. H., and Hoy, L. D., 1991, Geochemistry of hydrothermally altered rocks at the Horne mine, Noranda, Quebec: ECON. GEOL., v. 86, p. 506–528.

Munha, J., Barriga, F. J. A. S., and Kerrich, R., 1986, High ^{18}O ore-forming fluids in volcanogenic-hosted base metal massive sulfide deposits: Geologic $^{18}O/^{16}O$ and D/H evidence from the Iberian pyrite belt; Crandon, Wisconsin, and Blue Hill, Maine: ECON. GEOL., v. 81, p. 530–552.

Norton, D., and Taylor, H. P., 1979, Quantitative simulations of the hydrothermal systems of crystallizing magmas on the basis of transport theory and oxygen isotope data: An analysis of the Skaergaard intrusion: Jour. Petrology, v. 20, p. 421–486.

Paradis, S., Taylor, B. E., Watkinson, D. H., and Jonasson, I. R., 1993, Oxygen isotope zonation and alteration in the northern Noranda district, Quebec: Evidence for hydrothermal fluid flow: ECON. GEOL., v. 88, p. 1512–1525.

Parmentier, E. M., 1981, Numerical experiments on ^{18}O depletion in igneous intrusions cooling by groundwater convection: Jour. Geophys. Research, v. 86, p. 7131–7144.

Pisutha-Arnond, V., and Ohmoto, H., 1983, Thermal history, and chemical and isotopic compositions of the ore-forming fluids responsible for the kuroko massive sulfide deposits in the Hokuroku district of Japan: ECON. GEOL. MON. 5, p. 523–558.

SAS Inst. Inc., 1985, SAS user's guide: Statistics, version 5 edition: SAS Inst. Inc., 956 p.

Schiffman, P., and Smith, B. M., 1988, Petrology and oxygen isotope geochemistry of a fossil seawater hydrothermal system within the Solea graben, northern Troodos Ophiolite, Cyprus: Jour. Geophys. Research, v. 93, p. 4612–4624.

Setterfield, T. N., 1984, Nature and significance of the McDougall-Despina fault set, Noranda, Quebec: Unpub. M.Sc. thesis, Univ. Western Ontario, 157 p.

Spooner, E. T. C., Beckinsale, R. D., Fyfe, W. S., and Smewing, J. D., 1974, O^{18} enriched ophiolite metabasic rocks from E. Liguria (Italy), Pindos (Greece), and Troodos (Cyprus): Contr. Mineralogy Petrology, v. 47, p. 41–62.

Spooner, E. T. C., Beckinsale, R. D., England, P. C., and Senior, A., 1977a, Hydration, ^{18}O enrichment and oxidation during ocean floor hydrothermal metamorphism of the ophiolitic metabasic rocks from E. Ligura, Italy: Geochim. et Cosmochim. Acta, v. 41, p. 857–871.

Spooner, E. T. C., Chapman, J. J., and Smewing, J. D., 1977b, Strontium isotopic contamination and oxidation during ocean floor hydrothermal metamorphism of the ophiolitic rocks of the Troodos Massif, Cyprus: Geochim. et Cosmochim. Acta, v. 41, p. 873–890.

Taylor, B. E., and South, B. C., 1985, Regional stable isotope systematics of hydrothermal alteration and massive sulfide deposition in the West Shasta district, California: ECON. GEOL., v. 80, p. 2149–2163.

Taylor, H. P., 1974, Application of oxygen and hydrogen isotope studies to problems of hydrothermal alteration and ore deposition: ECON. GEOL., v. 69, p. 843–883.

Veizer, J., and Compston, W., 1976, $^{87}Sr/^{86}Sr$ in Precambrian carbonates as an index of crustal evolution: Geochim. et Cosmochim. Acta, v. 40, p. 905–914.

Vervoort, J. D., White, W. M., Thorpe, R. I., and Franklin, J. M., 1993, Postmagmatic thermal activity in the Abitibi greenstone belt: Evidence from whole-rock Pb isotope data, Noranda and Matagami districts: ECON. GEOL., v. 88, p. 1598–1614.

APPENDIX

Table of $\delta^{18}O_r$ Determinations Used in this Study

All $\delta^{18}O_r$ determinations used in this study are listed below together with the range and township locations of the site from which the sample was collected, the rock type and crystallinity of the sample where it was determined, and the laboratory that carried out the isotopic measurements (K = Krueger Inc., Cambridge, Massachusetts; N = Knauth, University of Arizona, Tucson, Arizona; S = Savin, Case Western Reserve University, Cleveland, Ohio). The sample column indicates where multiple samples were collected at the same site. Entries where site and sample are identical indicate replicate analyses.

Site	Sample	Range	Township	$\delta^{18}O_r$ (‰)	Rock type	Crystallinity	Laboratory
1001		43.38	56.32	6.44	1.0	1.0	K
1001	2	43.38	56.32	5.94	1.0	0.0	K
1001	3	43.38	56.32	6.07	1.0	1.0	S
1001	3	43.38	56.32	5.60	1.0	1.0	S
1001	3	43.38	56.32	6.63	1.0	1.0	S
1001	4	43.38	56.32	6.24	1.0	1.0	K
1005		42.35	56.44	5.94	2.0	1.0	K
1006		41.30	56.70	8.93	2.5	0.0	K
1006	7	41.30	56.70	7.84	2.5	0.0	K
1008		41.41	56.68	8.39	2.5	0.0	S
1008	9	41.41	56.68	9.13	2.5	0.0	K
1010		41.50	56.71	9.15	1.0	0.0	S
1010	11	41.50	56.71	8.04	1.0	0.0	K
1012		41.71	56.71	7.67	1.0	0.0	S
1014	C	40.84	56.55	7.10	1.0	0.0	S

Appendix (*Cont.*)

Site	Sample	Range	Township	$\delta^{18}O_r$ (‰)	Rock type	Crystallinity	Laboratory
1015	A	40.46	56.77	8.07	1.0	0.0	S
1016	A	40.13	56.92	5.73	1.0	0.0	K
1017		38.90	57.92	4.97			S
1018	C	38.25	58.08	6.44			S
1019		39.57	57.29	5.11	1.0	0.0	S
1020	B	39.23	58.75	4.24	1.0	0.0	K
1021	A	34.39	61.16	6.73	2.0	0.0	K
1021	B	34.39	61.16	9.93	2.0	0.0	K
1021	C	34.39	61.16	7.93	2.0	0.0	K
1021	D	34.39	61.16	8.33	2.0	0.0	K
1021	F	34.39	61.16	5.83	2.0	0.0	K
1022		34.29	61.23	4.89	2.0	1.0	S
1022		34.29	61.23	5.16	2.0	1.0	S
1023		35.62	62.47	10.84	1.0	0.7	K
1026	A	36.42	62.24	10.95	2.5	0.0	S
1027	A	30.48	60.84	7.90	1.0	0.0	K
1027	A	30.48	60.84	7.68	1.0	0.0	S
1028	A	30.66	61.29	5.69	1.0	0.0	S
1028	A	30.66	61.29	5.45	1.0	0.0	S
1028	A	30.66	61.29	5.70	1.0	0.0	S
1028	A	30.66	61.29	5.44	1.0	0.0	S
1028	A	30.66	61.29	5.46	1.0	0.0	S
1028	B	30.66	61.29	7.85	1.0	0.0	S
1028	B	30.66	61.29	7.60	1.0	0.0	S
1028	B	30.66	61.29	7.63	1.0	0.0	S
1028	B	30.66	61.29	7.52	1.0	0.0	S
1028	B	30.66	61.29	7.61	1.0	0.0	S
1028	B	30.66	61.29	7.60	1.0	0.0	S
1028	B	30.66	61.29	7.50	1.0	0.0	K
1028	C	30.66	61.29	6.44	1.0	0.0	S
1028	C	30.66	61.29	7.14	1.0	0.0	S
1028	C	30.66	61.29	7.11	1.0	0.0	S
1028	C	30.66	61.29	6.21	1.0	0.0	S
1028	C	30.66	61.29	7.11	1.0	0.0	S
1029	A	30.81	62.06	5.66	2.0	0.0	S
1030	A	31.15	62.66	5.00	1.5	0.0	K
1030	A	31.15	62.66	4.65	1.5	0.0	S
1030	B	31.15	62.66	4.64	1.5	0.0	S
1030	C	31.15	62.66	5.25	1.5	0.0	S
1030	C	31.15	62.66	4.35	1.5	0.0	S
1030	C	31.15	62.66	6.33	1.5	0.0	S
1030	C	31.15	62.66	5.06	1.5	0.0	S
1030	C	31.15	62.66	5.63	1.5	0.0	S
1031	A	31.23	62.91	4.23	1.0	0.0	S
1031	A	31.23	62.91	4.34	1.0	0.0	S
1032	A	31.07	63.69	7.54	2.5	0.0	S
1032	B	31.07	63.69	8.54	2.5	0.0	K
1032	B	31.07	63.69	7.95	2.5	0.0	S
1033		30.97	63.91	9.92	2.5	0.0	S
1033		30.97	63.91	9.20	2.5	0.0	S
1034	A	30.90	64.26	10.44	2.5	0.0	S
1034	B	30.90	64.26	9.88	2.5	0.0	S
1035	B	30.90	64.53	9.21	2.5	0.0	S
1036	A	30.83	64.75	10.68	2.5	0.0	S
1036	A	30.83	64.75	11.04	2.5	0.0	S
1036	A	30.83	64.75	10.62	2.5	0.0	S
1036	A	30.83	64.75	10.86	2.5	0.0	S
1036	A	30.83	64.75	10.60	2.5	0.0	K
1036	A	30.83	64.75	11.40	2.5	0.0	N
1036	B	30.83	64.75	9.25	2.5	0.0	S
1037	A	47.44	46.99	8.14	3.0	0.0	K
1038	A	47.62	47.19	7.63	2.5	0.0	K
1038	B	47.62	47.19	7.53	2.5	0.0	K
1039	A	47.80	47.44	8.30	2.0	0.0	K
1040	B	48.25	48.05	10.40	2.0	0.0	K
1041	A	48.28	48.39	9.40	1.0	0.0	K
1042	B	48.12	48.70	5.53	3.0	0.0	K
1043	A	48.19	48.87	10.50	2.0	0.0	K

Appendix (*Cont.*)

Site	Sample	Range	Township	$\delta^{18}O_r$ (‰)	Rock type	Crystallinity	Laboratory
1044	A	47.23	47.25	8.50	2.5	0.0	K
1046	B	45.48	47.22	6.64	2.5	1.0	K
1047	A	45.26	47.21	4.90	1.0	0.0	K
1047	C	45.26	47.21	5.40	1.0	0.0	K
1047	C	45.26	47.21	5.70	1.0	0.0	K
1049		44.00	47.66	4.83			K
1050		42.18	49.03	7.20	2.5	0.0	K
1051	C	42.80	48.55	7.80	1.0	0.5	K
1052	B	43.57	47.86	6.50			K
1053	B	40.90	48.02	4.72			S
1053	B	40.90	48.02	5.27			S
1054		39.71	48.01	6.05	1.0	0.0	S
1055	B	39.04	48.06	5.84	2.5	1.0	S
1056	A	38.74	47.92	5.80	2.5	1.0	S
1057	A	36.91	48.01	5.70	2.5	1.0	S
1058	B	34.89	47.94	6.35	2.5	1.0	S
1059	B	33.93	48.33	9.19	2.5	1.0	S
1060	A	32.99	49.88	6.93	2.5	1.0	S
1061	C	49.18	47.68	9.90	3.0	0.0	K
1062	A	50.46	46.98	9.10	−1.	0.0	K
1063	A	51.64	48.74	6.23	2.0	1.0	K
1064	A	52.63	51.65	8.33	3.0	0.2	K
1065	B	53.26	53.02	5.23	2.0	1.0	K
1066	A	46.22	55.14	9.80	2.5	1.0	K
1067	A	45.82	54.53	8.60	2.5	1.0	K
1068	B	45.17	52.51	6.80	2.5	1.0	K
1069	A	45.01	51.37	6.24	2.0	0.8	K
1070	A	43.62	51.78	6.40	2.0	1.0	K
1071	B	43.65	51.41	5.33	1.0	0.0	K
1072	B	43.80	51.09	6.14	1.0	0.0	K
1073	B	43.26	52.36	6.80			K
1074	B	43.01	52.36	7.80	1.0	0.0	K
1075	A	42.55	52.71	9.40	2.0	0.8	K
1076	A	40.38	51.68	4.90	2.0	0.8	K
1076	A	40.38	51.68	4.90	2.0	0.8	K
1076	A	40.38	51.68	4.00	2.0	0.8	K
1076	A	40.38	51.68	4.00	2.0	0.8	K
1077		41.31	52.41	4.54			K
1077	36	41.31	52.41	3.74	1.0	0.5	K
1077	79	41.31	52.41	5.04			K
1077	84	41.31	52.41	3.74	2.0	0.0	K
1077	86	41.31	52.41	4.04			K
1077	88	41.31	52.41	5.64			K
1077	91	41.31	52.41	4.54	1.0	0.0	K
1077	91	41.31	52.41	3.34	1.0	0.0	K
1077	92	41.31	52.41	4.44			K
1077	93	41.31	52.41	5.40			K
1077	94	41.31	52.41	5.10	2.0	0.0	K
1077	95	41.31	52.41	5.20	2.5	0.2	K
1077	96	41.31	52.41	4.90			K
1077	98	41.31	52.41	3.80			K
1077	99	41.31	52.41	4.70			K
1100		41.72	52.44	5.60	1.0	0.0	K
1101		21.87	65.67	5.95	2.0	1.0	S
1102	A	21.43	65.00	7.50	2.5	0.0	S
1103	A	21.60	63.99	6.63	2.5	0.0	S
1103	A	21.60	63.99	6.22	2.5	0.0	S
1103	B	21.60	63.99	6.65	2.5	0.0	S
1104	A	22.07	62.95	6.61	2.5	0.2	S
1105	A	23.58	62.40	8.93	2.5	0.0	S
1106	B	26.36	62.07	7.64	1.0	0.0	S
1107	B	28.28	61.64	5.52	1.0	0.2	S
1108	A	29.01	60.63	6.59	1.0	0.2	S
1108	C	29.01	60.63	7.71	1.0	0.2	S
1109	A	34.42	61.80	5.96	2.0	0.2	S
1110	B	34.64	61.95	4.85	1.0	1.0	S
1111		37.49	59.99	5.24	2.0	1.0	K
1111		37.49	59.99	5.54	2.0	1.0	K
1111	13	37.49	59.99	6.83	2.0	1.0	K

Appendix (*Cont.*)

Site	Sample	Range	Township	$\delta^{18}O_r$ (‰)	Rock type	Crystallinity	Laboratory
1111	14	37.49	59.99	6.73	2.0	0.8	K
1111	14	37.49	59.99	6.33	2.0	0.8	K
1111	16	37.49	59.99	8.73	2.0	0.2	K
1111	22	37.49	59.99	8.84	2.0	0.0	K
1123		46.17	56.48	9.53			K
1123		46.17	56.48	9.13			K
1123	24	46.17	56.48	8.70			K
1123	25	46.17	56.48	8.80			K
1123	26	46.17	56.48	6.60			K
1123	27	46.17	56.48	7.73			K
1123	28	46.17	56.48	7.14			K
1123	29	46.17	56.48	6.30			K
1123	30	46.17	56.48	7.33			K
1123	30	46.17	56.48	8.90			K
1123	31	46.17	56.48	6.90			K
1123	33	46.17	56.48	6.80			K
1123	34	46.17	56.48	6.04			K
1150	A	39.46	44.41	7.10			K
1151	B	39.95	44.50	7.20	1.0	0.0	K
2001		30.61	71.62	9.29	1.0	0.0	K
2002		30.61	71.61	6.97	2.0	0.0	S
2003		30.61	71.61	9.02	2.0	0.0	S
2003		30.61	71.61	9.02	2.0	0.0	S
2003		30.61	71.61	9.19	2.0	0.0	S
2003		30.61	71.61	9.19	2.0	0.0	K
2004		30.61	71.62	8.69	2.0	0.0	S
2005		30.21	70.82	7.54		0.0	S
2006		30.47	70.86	6.18	2.0	0.8	S
2006		30.47	70.86	5.75	2.0	0.8	S
2007		29.94	70.22	8.23	1.0	0.0	S
2008		30.10	69.74	8.34	1.0	0.0	S
2009		30.24	69.49	8.83	1.0	0.0	S
2010		30.10	68.91	7.06	1.0	0.0	S
2011		30.19	68.57	9.60	2.0	0.0	S
2012		30.16	67.83	9.68	1.0	0.0	S
2013		29.78	67.19	8.89	2.0	0.0	S
2014		29.80	66.84	7.53	1.0	0.0	S
2015		30.11	66.32	5.05	1.0	1.0	S
2015		30.11	66.32	5.38	1.0	1.0	S
2016		31.09	65.61	8.02	1.0	0.0	S
2016		31.09	65.61	8.03	1.0	0.0	S
2017		31.03	65.42	7.73	2.5	0.2	S
2018		31.01	65.28	8.95	3.0	0.0	S
2019		30.70	65.59	7.29	1.0	0.0	S
2020		29.95	65.76	8.67	3.0	0.0	S
2022		47.80	57.97	7.29	1.0	0.0	K
2023		47.96	57.98	8.30	2.5	0.0	K
2024		49.45	57.91	7.89	2.5	0.0	K
2025		57.74	63.14	7.29	1.0	0.0	K
2026		58.08	59.51	6.90	−1.	0.0	K
2027		58.04	58.69	5.89	−1.	0.0	K
2028		56.64	58.31	6.40	2.5	0.2	K
2029		55.69	58.19	5.20	−1.	0.0	K
2030		54.44	57.53	10.80	1.0	0.0	K
2031		53.73	58.12	8.00	1.0	0.0	K
2032		52.68	58.06	5.90	2.0	1.0	K
2033		51.18	57.99	7.30	2.0	1.0	K
2034		50.19	57.96	7.29	2.5	1.0	K
2034		50.19	57.96	7.69	2.5	1.0	K
2035		49.56	58.00	7.80	2.5	1.0	K
2036		46.34	57.22	8.50	1.0	0.5	K
2037		21.12	65.46	7.40	2.0	0.2	K
2038		20.65	65.53	6.70	2.0	0.2	K
2039		18.43	65.34	7.90	3.0	0.0	K
2040		17.26	65.32	7.40	2.0	0.0	K
2040		17.26	65.32	6.84	2.0	0.0	K
2041		16.53	65.66	9.13	2.5	0.0	K
2042		16.05	66.60	9.20	1.0	0.0	K

Appendix (*Cont.*)

Site	Sample	Range	Township	$\delta^{18}O_r$ (‰)	Rock type	Crystallinity	Laboratory
2043		15.55	67.49	8.90	1.0	0.2	K
2044		15.09	68.90	6.50	1.0	0.0	K
2045		14.61	69.94	7.10	1.0	0.0	K
2046		14.47	71.10	7.60	1.0	0.0	K
2047		14.34	71.56	8.20	1.0	0.0	K
2048		14.28	72.23	6.90	1.0	0.0	K
2049		26.39	69.88	9.50	2.5	0.2	K
2050		26.13	69.97	6.28	2.0	1.0	K
2051		26.33	69.55	8.70	2.5	0.2	K
2052		23.17	68.77	6.70	1.0	0.0	K
2053		24.45	68.60	6.70	1.0	0.2	K
2054		22.53	68.69	7.90	2.0	0.0	K
2055		22.82	67.35	7.00	1.0	0.2	K
2055		22.82	67.35	6.90	1.0	0.2	K
2056		23.17	66.97	5.70	2.0	0.8	K
2057		22.85	66.94	7.10	1.0	0.0	K
2058		22.21	66.71	8.08	2.0	0.8	K
2059		21.63	66.40	5.40	2.0	1.0	K
2060		21.25	66.51	6.28	2.0	1.0	K
2061		23.65	67.30	7.10	2.0	0.2	K
2062		24.90	67.80	8.88	2.5	1.0	K
2063		26.60	67.53	6.20	2.0	0.8	K
2064		25.20	67.07	7.00	1.0	0.0	K
2065		22.57	63.46	6.28	2.0	0.8	K
2066		23.93	64.55	5.78			K
2066		23.93	64.55	6.18			K
2067		24.36	66.25	8.98			K
2068		24.74	66.29	6.38			K
2069		25.68	66.83	6.88			K
2070		26.23	66.64	9.58			K
2071		26.96	66.13	10.84			K
2072		27.56	66.45	5.88			K
2073		28.37	66.74	9.78			K
2074		29.21	66.47	7.08			K
2075		28.46	62.24	6.18			K
2076		27.45	62.91	6.28			K
2077		27.62	64.50	8.98			K
2078		27.39	65.62	7.58			K
2079		21.47	62.74	9.58			K
2080		24.81	60.85	5.88			K
2081		24.70	60.25	7.24			K
2081		24.70	60.25	7.14			K
2082		24.35	59.92	7.94			K
2083		24.35	59.91	7.04			K
2084		23.84	59.67	7.44			K
2085		23.83	59.40	7.24			K
2086		24.00	58.91	8.24			K
2087		24.33	58.26	7.34			K
2088		24.96	56.26	5.64			K
2088		24.96	56.26	4.84			K
2088		24.96	56.26	4.84			K
2089		25.13	55.40	5.54			K
2090		25.13	55.40	5.14			K
2091		24.51	55.05	5.44			K
2091		24.51	55.05	4.84			K
2092		24.01	54.65	8.34			K
2093		23.98	54.08	7.34			K
2094		23.91	53.34	7.64			K
2095		24.62	53.17	7.74			K
2096		25.49	53.53	5.64			K
2096		25.49	53.53	6.34			K
2097		26.39	53.91	6.44			K
2098		29.17	54.12	5.34			K
2099		29.17	54.12	6.83			K
2100		31.79	52.55	7.24			K
2101		30.88	53.49	5.53			K
2102		39.79	56.23	7.13			K
2103		37.22	62.06	12.60		0.0	K
2104		38.46	64.51	11.00	1.0	0.2	K

Appendix (*Cont.*)

Site	Sample	Range	Township	$\delta^{18}O_r$ (‰)	Rock type	Crystallinity	Laboratory
2105		38.17	63.65	6.39	1.0	0.0	K
2106		37.43	62.75	7.70	2.0	1.0	K
2107		42.12	60.41	6.20	−1.	0.0	K
2108		41.29	60.60	6.90	1.0	0.0	K
2109		40.70	60.48	8.80		0.0	K
2110		46.94	58.39	10.39	2.0	0.0	K
2111		46.94	58.39	8.49	2.0	0.8	K
2112		46.87	59.20	8.29	2.0	0.2	K
2113		46.74	60.32	9.09	1.0	0.0	K
2114		45.66	61.74	9.99	−1.	0.0	K
2115		45.34	62.46	7.09	1.0	0.2	K
2116		44.19	64.62	8.19	1.0	0.0	K
2118		42.45	65.90	9.20	1.0	0.0	K
2119		41.88	65.98	9.90	1.0	0.0	K
2120		42.16	65.91	10.20	1.0	0.2	K
2121		42.53	66.51	11.70	1.0	0.0	K
2122		43.39	67.92	9.20	1.0	0.0	K
2123		44.02	68.44	7.60	2.0	0.8	K
2124		46.01	71.19	10.19	1.0	0.0	K
2125		45.70	72.11	8.99	−1.	0.0	K
2126		44.95	63.66	6.89	1.0	0.2	K
2127		37.95	56.11	2.34	1.0	0.0	K
2128		37.11	55.64	2.14	1.0	0.0	K
2128		37.11	55.64	1.64	1.0	0.0	K
2129		42.17	59.80	6.79	1.0	0.0	K
2130		42.47	59.50	8.89	2.0	0.0	K
2131		42.68	59.52	11.19	2.0	0.0	K
2132		42.96	59.49	6.89	1.0	0.0	K
2133		43.39	59.49	5.69	2.0	1.0	K
2134		43.64	59.54	10.19	2.5	0.0	K
2135		44.03	59.50	8.39	2.0	1.0	K
2136		44.54	59.60	9.29	2.0	0.0	K
2137		44.54	59.86	11.39	2.5	0.0	K
2138		44.57	60.15	14.09	2.0	0.2	K
2139		44.55	60.44	9.39	1.0	0.0	K
2140		38.83	60.10	10.50	2.0	0.2	K
2141		33.26	54.00	2.84			K
2142		33.73	54.96	5.94			K
2143		33.80	55.49	6.63			K
2144		33.87	56.28	5.14			K
2145		33.08	52.94	4.63			K
2146		47.59	43.43	7.33			K
2147		47.02	42.90	9.53			K
2147		47.02	42.90	9.73			K
2147		47.02	42.90	9.43			K
2148		46.98	41.19	8.83			K
2149		47.06	40.86	7.83			K
2150		46.19	39.92	6.03			K
2151		44.19	40.05	11.03			K
2152		43.35	40.05	11.13			K
2153		42.63	39.98	9.13			K
2154		41.63	39.93	7.33			K
2155		41.11	39.96	8.73			K
2156		46.83	40.07	7.93			K
2157		47.63	40.04	8.03			K
3001		51.59	40.36	11.00			K
3002		51.30	52.86	6.30			K
3003		50.15	48.91	6.10			K
3004		50.52	48.63	9.80			K
3005		49.34	48.37	9.20			K
3006		47.98	43.90	9.00			K
3007		47.83	43.90	10.30			K
3008		45.02	52.41	6.60			K
3009		44.44	52.37	5.20			K
3010		44.09	52.07	6.70			K
3011		43.33	51.93	5.50			K
3012		42.90	51.74	5.60			K
3013		43.83	51.39	6.50			K
3014		44.21	51.00	5.90			K

Appendix (*Cont.*)

Site	Sample	Range	Township	$\delta^{18}O_r$ (‰)	Rock type	Crystallinity	Laboratory
3015		44.22	50.96	5.90			K
3017		45.16	51.70	6.10			K
3018		45.68	50.13	8.30			K
3019		47.59	49.65	10.50			K
3020		45.18	51.20	5.60			K
3020		45.39	48.19	5.60			K
3021		46.93	47.54	8.00			K
3022		48.29	47.68	7.60			K
3023		46.54	55.63	6.40			K
3024		46.54	55.61	7.10			K
3025		43.93	64.43	8.60			K
3028		44.55	51.45	7.40			K
4001		33.71	43.11	5.90			K
4002		32.54	43.08	4.80			K
4003		31.92	43.11	11.70			K
4004		31.92	43.11	6.70			K
4005		34.79	43.13	5.00			K
4006		29.60	39.74	6.30			K
4007		28.48	40.40	10.60			K
4008		28.48	40.40	10.40			K
4009		29.34	40.72	9.70			K
4010		29.34	40.72	9.60			K
4011		29.26	41.22	11.30			K
4012		29.08	42.16	8.80			K
4013		28.43	42.64	7.60			K
4014		22.85	52.63	7.00			K
4015		21.86	52.17	11.30			K
4016		24.05	52.90	7.10			K
4017		24.09	52.70	7.70			K
4018		24.25	52.19	9.70			K
4019		24.06	51.92	8.70			K
4020		24.06	51.92	5.80			K
4021		24.06	51.92	8.60			K
4023		24.01	50.92	10.10			K
4024		23.95	50.39	6.00			K
4025		24.07	49.73	6.40			K
4026		24.57	49.85	5.40			K
4027		25.05	49.95	5.30			K
4028		25.50	49.80	7.90			K
4029		25.89	49.65	7.50			K
4030		25.89	49.65	3.20			K
4031		26.92	48.79	8.70			K
4032		26.94	47.84	5.70			K
4033		35.54	43.52	4.30			K
4034		35.00	42.85	9.40			K
4035		34.31	42.49	9.50			K
4036		33.05	41.43	6.20			K
4037		32.45	40.48	8.80			K
4038		30.61	39.86	9.10			K
4039		27.00	46.96	6.20			K
4040		27.21	46.11	5.90			K
4041		27.36	45.60	5.50			K
4042		28.26	42.97	10.20			K
4043		38.60	46.49	3.90			K
4044		37.21	46.47	5.60			K
4045		35.28	46.28	0.90			K
4046		34.25	46.37	5.50			K
4047		32.72	50.74	5.90			K
4048		31.80	52.42	5.80			K
4049		31.41	53.11	4.70			K
4050		30.84	53.46	7.10			K
4051		30.25	53.81	6.50			K
4052		29.57	54.00	5.60			K
4053		29.47	55.72	8.10			K
4054		29.30	56.34	8.00			K
4055		35.05	63.12	5.60			K
4056		34.56	62.27	11.60			K
4057		34.47	62.70	8.30			K
4058		34.08	63.40	9.50			K

Appendix (*Cont.*)

Site	Sample	Range	Township	$\delta^{18}O_r$ (‰)	Rock type	Crystallinity	Laboratory
4059		34.08	63.56	5.90			K
4060		34.08	64.25	10.10			K
4061		34.08	64.01	8.30			K
4062		36.96	61.74	10.40			K
4063		36.92	61.40	7.70			K
4064		36.94	61.27	7.50			K
4065		36.92	61.13	8.80			K
4066		36.91	60.91	8.50			K
4067		36.91	60.80	8.80			K
4068		37.09	60.32	5.50			K
4069		37.15	60.33	8.50			K
4070		41.13	59.01	9.80			K
4071		40.34	59.02	5.50			K
4072		39.75	59.00	3.70			K
4073		41.43	59.03	5.60			K
4074		41.69	58.18	5.30			K
4075		41.59	57.38	8.90			K
4075		41.59	57.38	9.10			K
4076		44.36	56.62	6.10			K
4077		45.95	48.14	7.00			K
4078		45.26	47.99	6.10			K
4079		46.00	48.85	8.30			K
4079		46.00	48.85	7.90			K
4080		46.83	49.38	9.00			K
4080		46.83	49.38	8.70			K
4081		47.31	49.53	11.00			K
4081		47.31	49.53	11.60			K
4082		46.16	44.37	7.40			K
4083		46.74	44.39	7.10			K
4084		48.04	43.91	9.70			K
4085		13.32	35.88	9.00			K
4086		49.73	44.49	9.30			K
4087		50.10	45.00	8.20			K
4088		50.33	45.51	10.50			K
4089		50.54	46.66	9.00			K
4090		44.79	45.31	6.50			K
4091		43.69	45.57	8.60			K
4092		39.02	42.69	12.10			K
4093		37.59	41.62	8.10			K
4094		40.88	41.53	7.70			K
4095		39.49	41.56	10.30			K
4096		39.49	41.55	10.60			K
4097		41.64	41.82	7.30			K
4098		43.56	42.14	8.50			K
4099		46.03	43.95	5.00			K
4100		38.82	49.28	5.00			K
4101		38.48	50.14	6.40			K
4102		38.77	51.11	6.40			K
4103		38.47	52.07	6.30			K
4104		38.44	52.49	6.90			K
4105		38.32	50.48	8.60			K
5001		61.94	58.94	12.7			K
5002		61.93	58.93	12.8			K
5003		61.96	58.92	11.8			K
5004		61.28	58.34	10.0			K
5006		60.53	58.33	8.0			K
5008		60.01	58.31	6.5			K
5009		60.02	58.31	6.1			K
5010		59.52	58.31	6.9			K
5011		59.49	58.33	7.6			K
5012		59.52	58.31	1.5			K
5013		59.52	58.32	6.7			K
5014		58.76	58.17	5.7			K
5015		58.62	57.74	1.3			K
5016		58.29	57.38	6.9			K
5017		58.73	56.89	3.4			K
5018		58.13	56.71	6.1			K
5019		57.40	56.83	5.2			K
5020		57.40	56.83	8.2			K

Appendix (*Cont.*)

Site	Sample	Range	Township	$\delta^{18}O_r$ (‰)	Rock type	Crystallinity	Laboratory
5021		57.22	56.66	8.6			K
5022		56.74	56.90	8.3			K
5024		56.75	56.88	4.7			K
5025		55.50	57.67	10.4			K
5027		55.36	57.30	6.8			K
5028		55.36	57.30	6.6			K
5029		54.66	56.06	7.9			K
5031		54.15	55.87	10.4			K
5032		53.13	56.65	7.1			K
5034		58.16	54.89	9.8			K
5035		56.80	54.78	9.8			K
5036		58.97	55.11	5.5			K
5037		60.00	55.17	7.5			K
5038		60.46	54.88	6.4			K
5039		60.60	54.84	8.2			K
5040		60.88	55.13	3.4			K
5041		62.58	55.08	8.5			K
5042		63.90	55.22	6.8			K
5043		34.79	47.12	5.5			K
5044		34.58	47.13	5.9			K
5045		34.89	45.87	2.3			K
5046		34.90	45.38	3.7			K
5047		35.02	45.05	3.4			K
5048		35.58	43.95	4.9			K
5049		35.57	43.92	0.6			K
5050		42.56	55.99	3.9			K
5051		42.38	55.48	4.5			K
5052		42.46	55.18	7.4			K
5053		42.26	55.18	5.6			K
5054		42.28	53.45	7.3			K
5055		42.81	57.02	8.0			K
5056		42.80	57.04	8.4			K
5057		42.78	56.62	6.8			K
5058		47.66	49.88	10.4			K
5059		47.47	50.32	11.2			K
5060		47.25	50.90	10.1			K
5061		47.46	51.44	8.8			K
5062		48.23	51.21	10.7			K
5063		47.85	51.98	8.6			K
5064		47.25	53.08	6.0			K
5065		47.68	53.89	7.0			K
5066		46.78	53.87	5.8			K
5067		47.20	54.79	7.4			K
5068		48.25	55.90	8.2			K
5069		47.60	55.97	8.5			K
5072		45.04	51.74	5.8			K
5073		45.03	51.72	5.3			K
5074		44.83	52.29	5.6			K
5075		45.11	53.19	5.9			K
5076		45.16	53.84	6.1			K
5077		34.98	52.54	6.7			K
5078		34.97	52.83	6.5			K
5079		34.94	53.17	6.8			K
5080		35.57	53.49	8.0			K
5081		36.48	54.23	8.0			K
5082		36.79	54.45	6.0			K
5083		34.43	56.88	6.2			K
5084		35.42	56.46	2.8			K
5084		35.03	56.71	7.3			K
5085		36.06	56.06	2.5			K
5086		36.43	55.76	4.7			K
5087		36.85	55.52	6.3			K
5088		37.12	55.34	6.0			K
5089		31.12	48.43	9.7			K
5090		31.46	48.58	8.0			K
5091		31.76	48.72	7.6			K
5092		32.47	49.04	7.0			K
5093		32.75	49.22	7.7			K

Appendix (*Cont.*)

Site	Sample	Range	Township	$\delta^{18}O_r$ (‰)	Rock type	Crystallinity	Laboratory
5094		33.38	49.61	7.1			K
5095		33.65	49.78	7.9			K
5096		33.99	50.04	6.1			K
5097		34.35	50.25	5.5			K
5098		33.14	49.43	6.3			K
5099		33.36	51.15	6.3			K
5100		32.82	50.79	6.1			K
5101		32.34	50.44	8.1			K
5102		58.42	54.52	7.9			K
5103		59.34	53.07	9.1			K
5104		59.69	52.97	10.2			K
5105		59.94	52.68	8.6			K
5106		60.34	52.55	6.1			K
5107		60.53	51.62	7.2			K
5108		60.90	50.88	10.7			K
5109		51.51	54.13	5.4			K
5110		53.00	55.59	8.1			K
5111		52.79	55.36	7.0			K
5111		52.80	55.36	7.1			K
5112		52.53	55.03	10.0			K
5114		51.19	47.46	9.4			K
5115		50.06	47.21	10.1			K
5116		50.28	43.43	6.0			K
5117		50.26	41.76	11.2			K